

Hybrid quantum-classical approach for combinatorial problems at hadron colliders

Zhongtian Dong,^{1,*} Taejoon Kim,^{2,†} Kyoungchul Kong,^{1,‡} Myeonghun Park,^{3,4,5,§} and Jacob L. Scott^{1,¶}

¹*Department of Physics and Astronomy, University of Kansas, Lawrence, KS 66045, USA*

²*School of Electrical, Computer and Energy Engineering,
Arizona State University, Tempe, AZ 85281, USA*

³*School of Physics, Korea Institute for Advanced Study, Seoul 02455, KOREA*

⁴*Institute of Convergence Fundamental Studies, Seoultech, Seoul 01811, KOREA*

⁵*School of Natural Sciences, Seoultech, Seoul 01811, KOREA*

In recent years, quantum computing has drawn significant interest within the field of high-energy physics. We explore the potential of quantum algorithms to resolve the combinatorial problems in particle physics experiments. As a concrete example, we consider top quark pair production in the fully hadronic channel at the Large Hadron Collider. We investigate the performance of various quantum algorithms such as the Quantum Approximation Optimization Algorithm (QAOA) and a feedback-based algorithm (FALQON). We demonstrate that the efficiency for selecting the correct pairing is greatly improved by utilizing quantum algorithms over conventional kinematic methods. Furthermore, we observe that gate-based universal quantum algorithms perform on par with machine learning techniques and either surpass or match the effectiveness of quantum annealers. Our findings reveal that quantum algorithms not only provide a substantial increase in matching efficiency but also exhibit scalability and adaptability, making them suitable for a variety of high-energy physics applications. Moreover, quantum algorithms eliminate the extensive training processes needed by classical machine learning methods, enabling real-time adjustments based on individual event data.

I. INTRODUCTION

Understanding the mysteries of nature at the smallest possible scales requires extraordinarily large and complex particle physics experiments. With the ongoing success of the Large Hadron Collider (LHC) at CERN, we can control $\mathcal{O}(10^{13})$ eV energy scale experiment to probe the physics at the length scale of $\mathcal{O}(10^{-19})$ m. While there are sound theoretical reasons to believe that new physics beyond the Standard Model is going to be revealed in those experiments, significant theoretical and experimental challenges lie ahead [1]. The future upgrade to the High-Luminosity LHC (HL-LHC) will boost the data delivery rate by 100-fold, reaching approximately 1 exabyte per year. This massive increase in event size, data volume, and complexity will introduce both quantitative and qualitative challenges, significantly stretching the limits of available computational resources. In this era of big data, a discovery in particle physics experiments will only be achievable through innovative methods for data collection, processing, and analysis [2].

Among many others, the combinatorial problems have become one of the central challenges in hadron collider physics analyses. Unlike lepton colliders, the environment at hadron colliders is significantly more complex, making these tasks even more difficult especially with events involving jets. In typical hadron collider events, numerous jets are present - some originating from the

decays of heavy particles, while others may result from the dynamics of quantum chromodynamics including initial/final state radiation (ISR/FSR). This complicates the event reconstruction process. The problem is exacerbated by detector limitations, such as finite resolution and the inability to determine properties of a parton which acts as the seed of a jet. These factors contribute to a significant combinatorics challenge: determining which of the many jets in an event is the correct one to associate with a specific particle decay.

Solving the combinatorial problem enhances the precision in the measurement of particle properties and expedites the discovery of new physics [3]. Many kinematic methods as well as machine learning (ML) methods have been proposed. Only recently have studies begun to explore specific machine learning methods - particularly those that leverage the permutation-invariant structure of attention-based neural networks - to address the combinatorial problems in the fully hadronic channel [4–6] and dilepton [7] channel for $t\bar{t}$ production. See [2, 7] for references on kinematics and feature engineering for collider phenomenology.

In this paper, we go beyond the classical machine learning methods and explore various universal quantum algorithms to resolve the combinatorial problems. Taking the fully hadronic $t\bar{t}$ production as a concrete example, we examine the performance of hybrid quantum-classical algorithms, including the Quantum Approximation Optimization Algorithm (QAOA) [8], its variants [9, 10], and the feedback-based algorithm FALQON [11]. We compare their results to the performance of quantum annealing [12] and kinematic approaches like the hemisphere method [13, 14].

There are a few ways to assess the performance of algorithms utilizing quantum circuits [15, 16]: the number

* cdong@ku.edu

† taejoonkim@asu.edu

‡ kckong@ku.edu

§ parc.seoultech@seoultech.ac.kr

¶ jacob.scott@ku.edu

of adjustable parameters, convergence of accuracy and loss, the number of gates used, the computational complexity, etc. In this paper, we will focus on the accuracy of various algorithms, *i.e.*, how well we can identify the correct combination. We find that the efficiency (or the matching accuracy) in selecting the correct pairing is enhanced when using quantum algorithms compared to conventional kinematic methods.

This paper is structured as follows. In section II, we review quantum optimization briefly and introduce the problem Hamiltonian that we study in this article. In section III, we describe preparation of the data set. We provide a short review on quantum algorithms that we use to resolve the combinatorial problem and show results for each method in section IV. In section V, we compare performance of different algorithms altogether. Section VI is reserved for summary and outlook. In appendices, we provide schematic diagrams on quantum circuits (appendix A) and discuss effects of quantum noise (appendix B). We make short comments on detector effects (appendix C), performance of quantum algorithms for different processes with the same final state (appendix D) and quantum algorithms based on a non-adiabatic path (appendix E).

II. QUANTUM OPTIMIZATION AND COLLIDER ANALYSES

Optimization problems are ubiquitous appearing across a wide range of fields and applications. Often classical optimization methods struggle due to the complexity or size of the problem. These are often problems that are computationally intensive, difficult to solve exactly, or have exponentially growing solution spaces as the problem size increases. This is where quantum optimization is particularly useful [17]. Recently, the exploration of various quantum algorithms in high energy physics research has gained attention [18]. Examples include parton showers [19–22], jet clustering [23–29], reconstruction of particle tracks [30], application in lattice field theory [31], new physics searches [32], etc. We refer to Refs. [33–39] for more details on quantum computing in high energy physics phenomenology.

Hybrid quantum-classical algorithms are particularly valuable for various optimization problems, especially for those that are difficult or intractable for classical algorithms alone. These algorithms combine the strengths of quantum computing with classical methods to solve complex problems more efficiently [40–42]. Variational quantum algorithms (VQAs) are one special type of quantum circuit with adjustable parameters, which would be obtained via classical optimization procedures. It is important to note that these adjustable parameters in quantum algorithms differ from the learnable parameters used in machine learning approaches.

Hybrid quantum-classical algorithms optimize parameters for each input without the need for a training pro-

cess, which means they do not face generalization issues like those seen in modern classical machine learning (ML) algorithms. This is particularly useful in high energy physics analysis, since classical ML algorithms rely on Monte Carlo (MC) simulations at various stages (parton-level, hadron-level, and detector-level) during training, leading to generalization challenges because the test samples come from collider data and MC simulations are imperfect. In contrast, algorithms based on quantum circuits adjust parameters for each individual event, eliminating the need for training.

Recent theoretical studies have shown that VQAs are more expressive than classical neural networks [43–46] with respect to the number of parameters or the learning speed. In particular, numerical simulation in Refs. [47–54] demonstrated that some hybrid quantum-classical architectures reach accuracy higher than conventional neural networks with similar number of training parameters.

In particular, quadratic unconstrained binary optimization (QUBO) problems are studied in depth for many reasons [55–57]. For one, QUBO appears ubiquitously across science - in social networks, engineering, and physics, among other fields. In physics, it is known as the Ising model. Additionally, there are specialized quantum devices, that is the quantum annealer (QA), designed to solve QUBO problems [58, 59]. However, it is widely recognized that the quantum annealer performs poorly in cases with a degenerate spectrum [60], leading to the development of several algorithms for universal quantum computers [8, 9].

Interestingly, the combinatorial problems at particle physics experiments can be recast into a QUBO problem, and the complex environment at hadron colliders is an excellent playground to test such proposals [12]. Combinatorial problems at colliders are notorious and forbid full reconstruction of final states, which is essential to understand the underlying physics associated with the events.

To introduce the problem Hamiltonian, let us consider the production of two particles A and B at the LHC via a $2 \rightarrow 2$ process with their subsequent decays: $pp \rightarrow AB \rightarrow (j_1^A \cdots j_{n_A}^A)(j_1^B \cdots j_{n_B}^B)$, where A (B) decays into n_A (n_B) jets and $n = n_A + n_B$ is the total number of observed jets in the final state. We assume no initial state radiation (ISR) for this discussion¹. Then, the combinatorial problem (assigning each daughter particle to either A or B) becomes a binary classification, whose computational complexity increases exponentially as $\mathcal{O}(2^n)$. Note that the computational complexity of the quantum annealer is known to be $\mathcal{O}(n^2)$ for the same problem [12].

Given that no further assumptions are made, we need to define a guiding criterion to assign observed particles to the decay products of either A or B . Inspired by

¹ Ref. [12] chooses the first six hardest jets after full reconstruction with parton shower and hadronization.

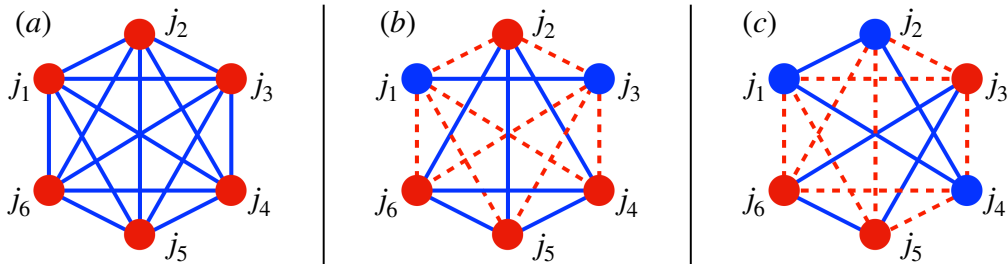


FIG. 1. Illustration of the QUBO problem considered in this paper as a fully connected graph. Each node represents a particle originating from the decay process of a specific parent particle. Red nodes represent particles from particle A , while blue nodes are from particle B . In our example of the $t\bar{t}$ process, there would be six hard jets resulting from the decay of the two top quarks. For example: (a) all particles originate from A , (b) $\{j_2, j_4, j_5, j_6\} \subset A$, $\{j_1, j_3\} \subset B$, and (c) $\{j_3, j_5, j_6\} \subset A$, $\{j_1, j_2, j_4\} \subset B$. The value of the edge connecting nodes i and j is given by $J_{ij} + (1/2)\lambda P_{ij}$. Edges connecting nodes from the same parent particle contribute positively to H_P and are shown as solid (blue) lines, while edges connecting nodes from different parent particles contribute negatively to H_P and are represented by dashed (red) lines. The task of finding the correct combinatorics is equivalent to identifying the graph configuration that minimizes H_P .

the general ‘minimum energy principle’ in physics, one might first consider minimizing the total invariant mass. However, this approach leads to a trivial partonic total energy for all visible particles and does not resolve the combinatorial issue [12]. A more viable alternative is to focus on the mass difference between A and B ,

$$H_0 = (P_1^2 - P_2^2)^2. \quad (1)$$

Here the four momenta of two mother particles A and B are defined as

$$P_1 = \sum_{i=1}^n p_i x_i, \quad (2)$$

$$P_2 = \sum_{i=1}^n p_i (1 - x_i), \quad (3)$$

where $x_i \in \{0, 1\}$ is an indicator variable: $x_i = 1$ if particle i with momentum p_i is from the particle A , otherwise it is 0. Using the substitution $x_i = (1 + s_i)/2$ with $s_i = \pm 1$, the problem Hamiltonian in Eq. (1) can be written as

$$\begin{aligned} H_0 &= \left(\sum_{ij} P_{ij} x_i x_j - \sum_{ij} P_{ij} (1 - x_i)(1 - x_j) \right)^2 \\ &= \left(\frac{1}{4} \sum_{ij} P_{ij} [(1 + s_i)(1 + s_j) - (1 - s_i)(1 - s_j)] \right)^2 \\ &= \left(\sum_{ij} P_{ij} s_i s_j \right)^2 = \sum_{ij} J_{ij} s_i s_j, \end{aligned} \quad (4)$$

where $P_{ij} = p_i \cdot p_j$ and $J_{ij} = \sum_{k\ell} P_{ik} P_{j\ell}$.

The target cost function H_0 in Eq. (1) is optimized for $m_A = m_B$, which corresponds to the many conventional new physics searches at the LHC. While H_0 can serve

as a useful starting point, it must be generalized to accommodate more complex scenarios, such as asymmetric production and off-shell effects. This can be achieved by introducing an additional term [12]

$$\begin{aligned} H_1 &= (P_1^2 + P_2^2) \\ &= \frac{1}{4} \sum_{ij} P_{ij} [(1 + s_i)(1 + s_j) + (1 - s_i)(1 - s_j)] \\ &\rightarrow \frac{1}{2} \sum_{ij} P_{ij} s_i s_j, \end{aligned} \quad (5)$$

with the dropping of a constant term $(1/2)(P_1 + P_2)^2$. The full cost function or full (problem) Hamiltonian becomes

$$H_P = H_0 + \lambda H_1, \quad (6)$$

where λ is a hyperparameter to be chosen during a optimization procedure. Ref. [12] suggests $\lambda = \frac{\min(J_{ij})}{\max(P_{ij})}$ to ensure similar weights for the two terms. Unless otherwise stated, we will use Eq. (6) in this study to estimate the performance of various quantum algorithms.

Then the optimization procedure will return a specific assignment of particles which minimizes the cost function or the problem Hamiltonian, therefore resolving the combinatorial problem. We will apply this idea for the fully hadronic channel of the top quark pair production, as shown in Fig. 1. Here, each circle (node) represents a particle, with particles of the same color belonging to the same group. The lines connecting two nodes indicate non-zero $J_{ij} + (1/2)\lambda P_{ij}$ coefficients in the QUBO model, illustrating a dense network. Here, the self-loop is ignored as its contribution to H_P remains constant. The objective is to correctly identify two groups, each containing three nodes—one group in red and the other in blue.

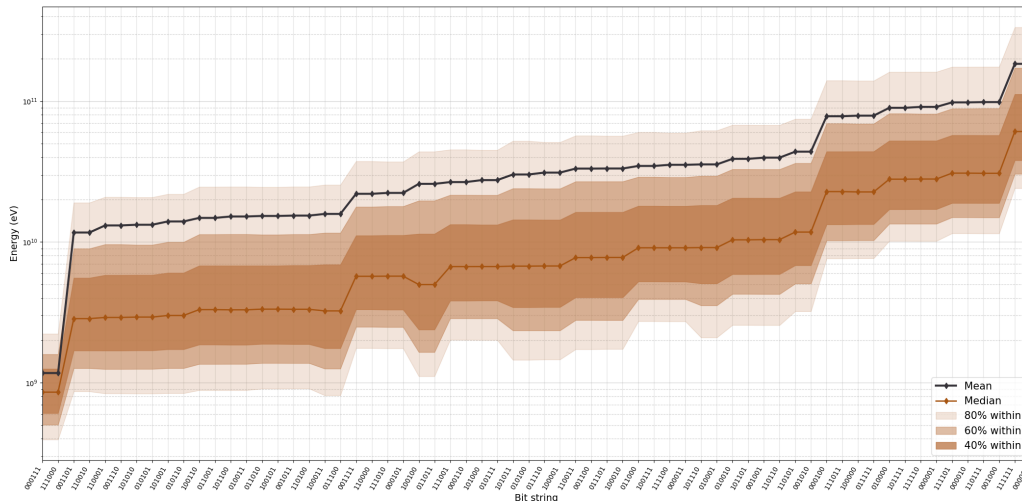


FIG. 2. The energy spectrum of the full Hamiltonian in Eq. (6) for parton-level events.

III. DATA PREPARATION

We generate parton-level events for top quark pairs in the fully hadronic channel using `MadGraph5_aMC@NLO` [61] at the 13 TeV LHC. Offshell effects of the top quark and W boson are taken into account properly. Basic cuts of $p_T > 25$ GeV, rapidity $|\eta| < 2.5$ and $\Delta R(j, j) > 0.4$ are imposed for the parton-level events. We will use these parton-level events to present the main results and compare against the kinematic methods. Results with detector effects and more realistic simulation are discussed in Appendix C.

Note that there are 6 jets ($n = 6$) in this study and therefore a total of 64 possible states. Since there are always two degenerate solutions (swapping $A = t$ and $B = \bar{t}$ with $n_A = 3$ and $n_B = 3$), the computational complexity in this case will be $2^{n-1} = 2^5$. For a given event, one can compute the values of the cost function for all possibilities, and declare the combination which leads to the smallest possible value (ground state) as the solution to the combinatorial problem.

Fig. 2 illustrates the energy value of the full Hamiltonian in Eq. (6) for 250k parton-level events. The states $(x_1 x_2 x_3 x_4 x_5 x_6)$ are ordered by the value of the energy spectrum such that the far-left corresponds to the ground state and the far-right state gives the largest energy value. In this case, the ground state is given by $(x_1 x_2 x_3 x_4 x_5 x_6) = (000111)$, which implies that $P_1 = p_4 + p_5 + p_6$ for top quark $t = (j_4 j_5 j_6)$ and $P_2 = p_1 + p_2 + p_3$ for anti-top quark $\bar{t} = (j_1 j_2 j_3)$. The energy spectrum clearly shows the substantial energy difference between the two lowest states.

Taking the ground state, one can compute the masses of t and \bar{t} , which are shown in the left-panel of Fig. 3. As expected, most events are populated at the correct

mass with very little spread due to the offshell effects of top quark and W boson (left-panel). Our study shows that 98.4% of the time the ground state is given by the symmetric configuration (3 for top and 3 for anti-top), while 1.6% of the time, 2 or 4 particles make up top quark (4 or 2 for anti-top quark) due to the finite width effects, as shown in the right panel of Fig. 3. The overall efficiency of resolving the combinatorial problem is about 79%

We also show results in Fig. 4 for the standard hemisphere method [13, 14] when applied to our event topology. In the hemisphere method, one clusters the visible particles into two groups trying to keep the invariant mass of each cluster to a minimum. In our example with 6 jets from the top quark production, we begin with two hardest jets assigned in A and B . The third jet is assigned to the side which leads to the smaller invariant mass. One repeats the same process for all remaining jets. We find that the overall efficiency of resolving the combinatorial problem with the hemisphere is about 36%. Comparing against results in Fig. 3, how can we improve the mass resolution in the left panel and the correct jet assignment in the right panel of Fig. 4? One can attempt to further improve on the hemisphere algorithm with suitable cuts on the invariant mass or the jet p_T by excluding certain reconstructed objects from the clustering algorithm [62]. In this paper we would like to investigate a different approach using quantum algorithms.

Whether or not the ground state resolves the combinatorial problem, Figs. 2 and 3 are the best results with the given choice of the Hamiltonian. Now we will investigate various algorithms to find this ground state in the next sections. We will present our results in terms of reconstructed mass, the jet-assignment and the success

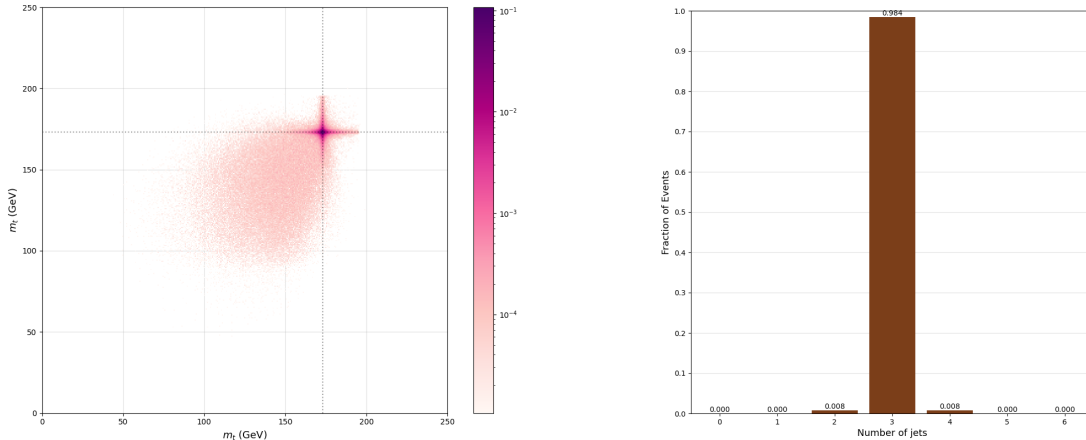


FIG. 3. The reconstructed masses (left) and jet-assignment (right) for parton-level events using the true ground state of the full Hamiltonian. The overall efficiency of resolving the combinatorial problem is about 79%.

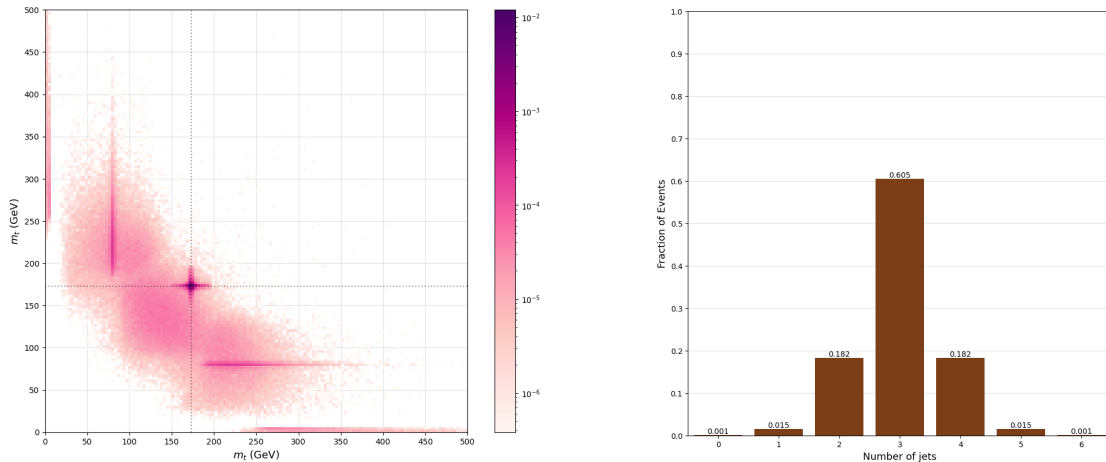


FIG. 4. The same as Fig. 3 but for the hemisphere method. The overall efficiency (matching accuracy) is about 36%.

rate.

IV. BRIEF REVIEW ON ALGORITHMS USED IN THIS PAPER

Variational quantum algorithms (VQAs) are a hybrid quantum-classical approach in which the parameters are adjusted using classical optimization techniques. For parameters θ , the circuit produces the state $|\theta\rangle$ with the goal of minimizing $\langle\theta|C|\theta\rangle$ where C is the cost function. As an example, if C is a Hamiltonian, then we are parameterizing the circuit to find the minimum energy eigenstate of the Hamiltonian. In this section, we briefly introduce two classes of quantum-classical algorithms: variational quantum algorithms based on QAOA [8] and the feedback-based algorithm FALQON [11]. All of our quantum algorithms are simulated with PennyLane [63]

and all code is available on [GitHub](https://github.com)². We use Adam optimizer [64] to optimize the parameters of variational algorithms. We used 12k events for the results presented in sections IV and V and Appendices, unless otherwise stated.

A. Quantum Approximation Optimization Algorithm (QAOA)

The Quantum Approximation Optimization Algorithm (QAOA) [8] is one of the most widely known VQAs. We

² https://github.com/crumpstrr33/collider_combinatorics_with_QAs

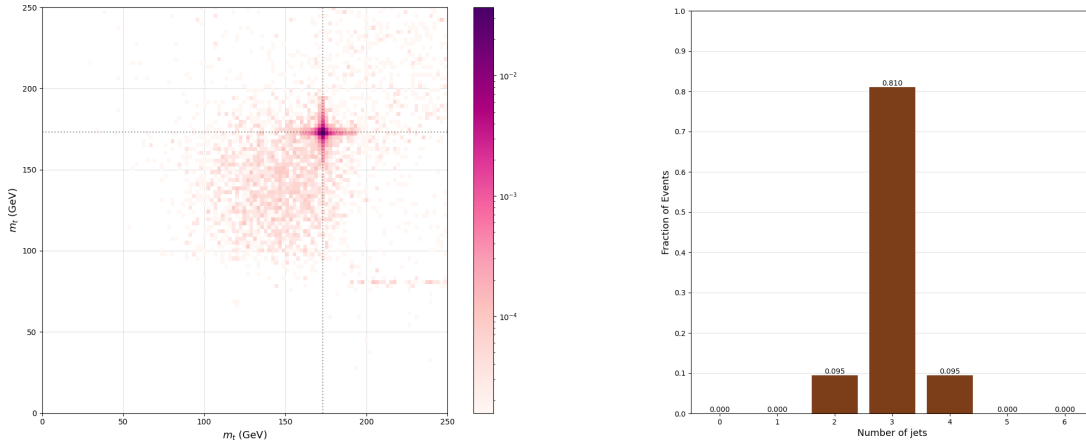


FIG. 5. The reconstructed masses (left) and jet-assignment (right) for parton-level events using QAOA with depth $p = 8$. The ground state is found for the full Hamiltonian. The overall efficiency (matching accuracy) is 55%.

consider the Hamiltonian of the form

$$H(t) = (1 - a(t)) H_M + a(t) H_P \quad (7)$$

where $a(0) = 0$ and $a(T) = 1$ for the final time T . Therefore, the full Hamiltonian transitions from being H_M initially to H_P where H_M is called the *mixer* Hamiltonian and H_P is the *problem* Hamiltonian. The former is a system that is easily solvable and preparable. We use

$$H_M = \sum_{i=1}^n \sigma_i^X, \quad (8)$$

where $\sigma_i^X = X_i$ is the Pauli X gate operating on the i -th qubit. The latter is a system with an energy eigenstate, specifically the ground state, which represents the solution to the given problem. Therefore, minimizing the cost function corresponds to finding the lowest eigenvalue.

We assume that the system begins with the Hamiltonian H_M and evolves into the Hamiltonian H_P slowly enough such that the adiabatic theorem is applicable. The time-evolution operator can be broken up into steps:

$$\begin{aligned} U(T, 0) &= U(T, T - \Delta t) U(T - \Delta t, T - 2\Delta t) \cdots U(\Delta t, 0) \\ &= \prod_{j=1}^p U(j\Delta t, (j-1)\Delta t) \end{aligned} \quad (9)$$

where $\Delta t = T/p$. If we consider Δt to be small, i.e. p is large, then we can approximate the time-evolution operator as follows with constant H over the short time interval Δt :

$$\begin{aligned} U(T, 0) &\approx \prod_{j=1}^p e^{-i\Delta t H(j\Delta t)} \\ &= \prod_{j=1}^p \exp \left[-i\Delta t [(1 - a(j\Delta t)) H_M + a(j\Delta t) H_P] \right]. \end{aligned} \quad (10)$$

Using the approximation $e^{\varepsilon(A+B)} = e^{\varepsilon A} e^{\varepsilon B} + \mathcal{O}(\varepsilon^2)$ for non-commuting operators A and B , The time-evolution operator can be rewritten as

$$\begin{aligned} U(T, 0) &\approx \prod_{j=1}^p \exp \left[-i\Delta t (1 - a(j\Delta t)) H_M \right] \\ &\quad \times \exp \left[-i\Delta t a(j\Delta t) H_P \right]. \end{aligned} \quad (11)$$

Note that for $\Delta t \rightarrow 0$ we get back $U(T, 0)$ exactly. Introducing $\beta_j \equiv \Delta t (1 - a(j\Delta t))$ and $\gamma_j \equiv \Delta t a(j\Delta t)$, we obtain

$$U(T, 0) = \prod_{j=1}^p \exp \left[-i\beta_j H_M \right] \exp \left[-i\gamma_j H_P \right]. \quad (12)$$

Defining the unitary operator $U(\alpha, H) \equiv \exp[-i\alpha H]$, the time-evolution operator can be written as

$$U(T, 0) = \prod_{j=1}^p U(\beta_j, H_M) U(\gamma_j, H_P) \quad (13)$$

which is exact in the limit $p \rightarrow \infty$. Then the quantum state initialized in the eigenstate of H_M , $|+\rangle^{\otimes n}$, evolves into the following final state

$$|\beta, \gamma\rangle = \sum_{j=1}^p U(\beta_j, H_M) U(\gamma_j, H_P) |+\rangle^{\otimes n}, \quad (14)$$

where $\beta = (\beta_1, \dots, \beta_p)$ and $\gamma = (\gamma_1, \dots, \gamma_p)$. Minimizing the expectation value of H_P

$$\langle H_P \rangle = \langle \beta, \gamma | H_P | \beta, \gamma \rangle, \quad (15)$$

is then the work of a classical optimizer. Having returned updated values for β and γ , the circuit is reran

and the process repeated. The schematic QAOA diagram of depth p for n qubits is shown in Fig. 11 of Appendix A, where $U(\beta, H_M)$ and $U(\gamma_i, H_P)$ are shown in Fig. 12 and Fig. 13, respectively.

Fig. 5 shows results on the reconstructed masses (left) and jet-assignment (right) for parton-level events using QAOA with depth $p = 8$. The ground state is found for the full Hamiltonian. Our model for the combinatorial problem is somewhat dense, since all coefficients are non-zero, $J_{ij} \neq 0$, although this particular problem requires 6 qubits. In general, a large number of layers is needed for dense models, while one can find fast and exact solution for sparse models [65].

There are many studies which extend this framework to allow alternation between more general families of operators [9, 66, 67]. The essence of this extension, the quantum alternating operator ansatz, is the consideration of general parameterized families of unitary transformations rather than only those corresponding to the time evolution under a fixed local Hamiltonian for a time specified by the parameter [68]. We will introduce a few variations which are relevant for our study in next subsections.

B. Multi-Angle QAOA

Multi-angle QAOA (ma-QAOA) [69] addresses an issue with the large depth (high p) usually needed for good results when using QAOA by increasing the number of adjustable parameters effectively shifting the burden from the quantum computer to the classical optimizer. In QAOA, there are $2p$ parameters with one parameter per each unitary operation per layer. Instead, in ma-QAOA, we allow each qubit to have its own free parameter, increasing the number from $2p$ to $(n + m)p$ where n is the number of qubits (the number of jets in this paper) and m depends on the form of H_P . The unitary for H_M for layer j then becomes

$$U(\beta_j, H_M) = \exp \left[-i \sum_{i=1}^n \beta_{ji} \sigma_i^X \right]. \quad (16)$$

See Fig. 14 in Appendix A for the mixer layer of layer i of ma-QAOA for n qubits. Similarly for $U(\gamma_j, H_P)$ we use

$$U(\gamma_j, H_P) = \exp \left[-i \sum_{k < \ell = 1}^n \gamma_{jkl} \sigma_k^Z \sigma_\ell^Z \right]. \quad (17)$$

Here, β_{ji} and γ_{jkl} are the adjustable parameters. For the Ising model Hamiltonian (QUBO type), we expect $m = \binom{n}{2}$ as every pair of qubits will have a 2-qubit gate. The ma-QAOA enhances the expressibility of each qubit, enabling greater flexibility to explore its Bloch sphere, which in turn allows the circuit to cover a larger portion of the Hilbert space. Fig. 6 shows results which

are greatly improved. The jet assignment changed from 80% (QAOA) to $\sim 99\%$ (ma-QAOA), thus improving the resolution of the reconstructed masses.

C. Expressive QAOA

Expressive QAOA (XQAOA) [70] builds upon ma-QAOA by adding another mixer Hamiltonian of Y gates such that

$$|\alpha, \beta, \gamma\rangle = \sum_{j=1}^p U(\alpha_j, H_X) U(\beta_j, H_M) U(\gamma_j, H_P) \quad (18)$$

where

$$U(\alpha_j, H_X) = \exp \left[-i \sum_{i=1}^n \alpha_{ji} \sigma_i^Y \right]. \quad (19)$$

Here $\sigma_i^Y = Y_i$ is the Pauli Y gate operating on the i -th qubit. This increases the number of adjustable parameters to $(2n + m)p$. The motivation for XQAOA is that it offers a higher expressibility still than ma-QAOA due to the addition of a Y gate rotation on top of the X gate. ma-QAOA is recovered when $\alpha = 0$.

The original QAOA is equivariant under the parity, $P = \sum_{i=1}^n X_i$, making the model learn the data better than non-equivariant models [52, 53, 71]. Inclusion of Y gates breaks equivariance of the quantum circuit but increases the expressivity [72]. As a result, a smaller depth leads to a better optimization for $p \leq n$. However, in our exercise, we have obtained results very similar to those using ma-QAOA and haven't noticed a significant improvement over ma-QAOA.

D. Feedback-based ALgorithm for Quantum OptimizatioN (FALQON)

Feedback-based ALgorithm for Quantum OptimizatioN [73] (FALQON) differs from the algorithms above as it eschews the use of the classical optimizer. The circuit layers are built recursively wherein, with each layer being parameterized by a single number, the layer's parameter is determined by the previous layers, inspired by quantum Lyapunov control [74]. In this algorithm, we begin with a Hamiltonian of the form $H(t) = H_P + \beta(t)H_M$ where $\beta(t)$ is called the control function. As before, we wish to find the minimum energy eigenstate of H_P and thus, for a state $|\psi(t)\rangle$, we require that

$$\frac{d}{dt} \langle \psi(t) | H_P | \psi(t) \rangle \leq 0 \quad \text{or} \quad (20)$$

$$\beta(t) \langle \psi(t) | i[H_M, H_P] | \psi(t) \rangle \leq 0. \quad (21)$$

There is a freedom at choosing what $\beta(t)$ is but it can be set as a feedback loop.

$$\beta(t) = -A(t - \tau), \quad (22)$$

$$A(t) \equiv \langle \psi(t) | i[H_M, H_P] | \psi(t) \rangle, \quad (23)$$

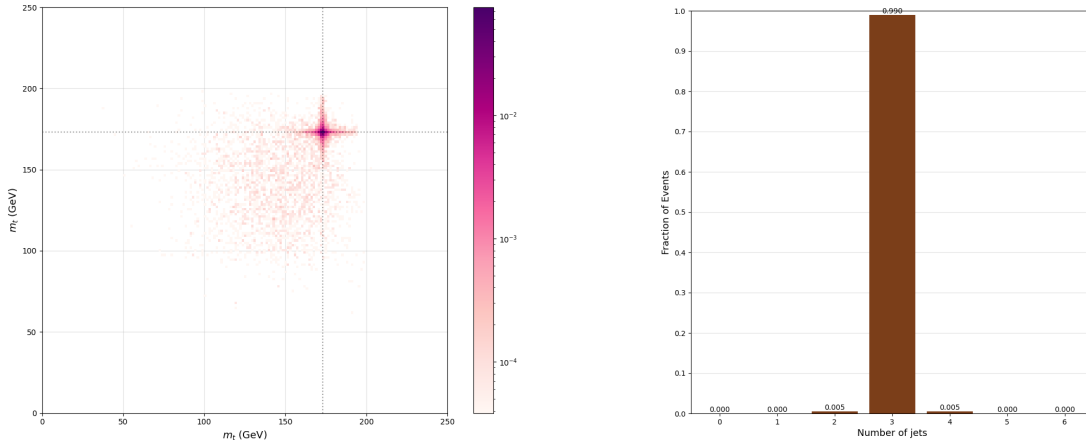


FIG. 6. The same as Fig. 5 but for ma-QAOA with $p = 8$. The overall efficiency (matching accuracy) is 75%.

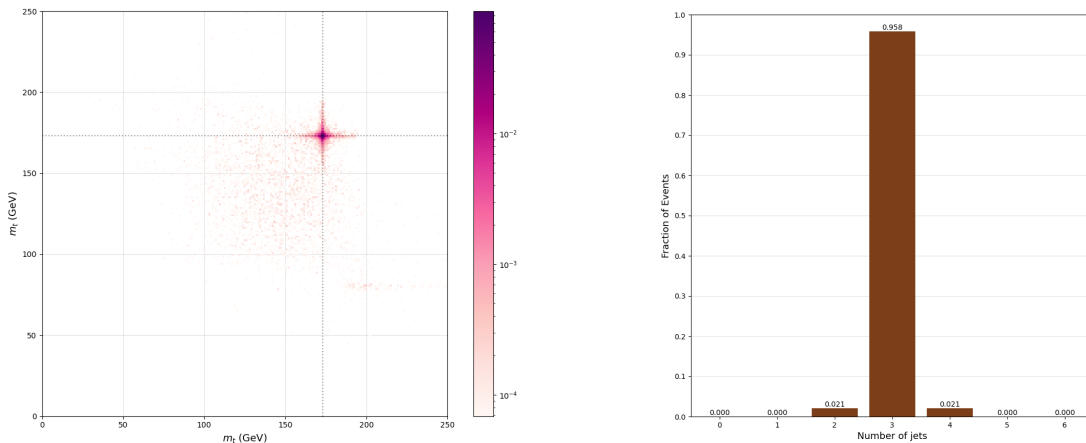


FIG. 7. The same as Fig. 5 but for FALQON with $p = 250$. The overall efficiency (matching accuracy) is 72%.

where τ is a small time delay. Following a similar derivation as above and discretizing time into time steps Δt , we obtain the recursive relationship $\beta_{k+1} = -A_k$ where $A_k = \langle \psi_k | i[H_M, H_P] | \psi_k \rangle$ and $|\psi_k\rangle$ is the quantum state of the circuit after the k -th layer:

$$|\psi_k\rangle = U_M(\beta_k)U_P |\psi_{k-1}\rangle, \quad (24)$$

where

$$U_M(\beta_k) = e^{-i\beta_k \Delta t H_M}, \quad \text{and} \quad U_P = e^{-i\Delta t H_P}. \quad (25)$$

Unlike the alternative versions (ma-QAOA or XQAOA) of QAOA which try to leverage the classical optimizer more, FALQON removes the optimizer entirely instead relying on expectation values of the operator $i[H_M, H_P]$ to build the circuit. Once the initial value of $\beta(t)$, $\beta(0) = \beta_1$, is chosen, the only parameters are Δt and the total number of layers p . (See Fig. 15 for a circuit diagram.)

Fig. 7 summarizes our results on the reconstructed masses and the jet assignment, which are comparable to those using ma-QAOA, outperforming conventional QAOA. We obtained the results with $\Delta t = 0.08$ and initial parameter $\beta_1 = 0$ for $p = 250$. We observe that our results are intensive to the initial value. A smaller Δt converges slower, while a larger Δt did not converge. Feedback-based quantum optimization algorithms are advancing rapidly; for recent developments and additional references, see [75–78].

V. COMPARISON OF DIFFERENT ALGORITHMS

We have briefly reviewed VQAs (QAOA and its variants, ma-QAOA and XQAOA) as well as a feedback

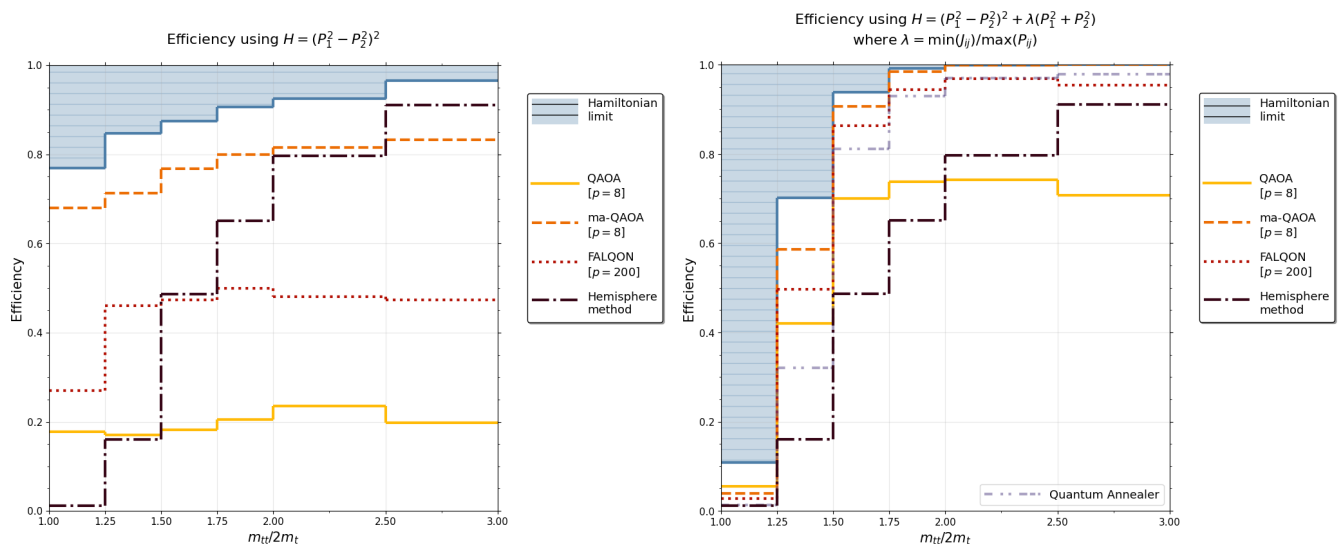


FIG. 8. The matching accuracy or efficiency of QAOA (solid, yellow), ma-QAOA (dashed, orange), FALQON (dotted, red) and hemisphere (purple, dot-dashed) for parton-level events for using H_0 only in Eq. (1) (left) and using $H = H_0 + \lambda H_1$ in Eq. (1) and Eq. (5).

based algorithm (FALQON). In this section, we present all results as a function of the boostness of the mother particles (two top quarks) [12], since boosted particles lead to the collimated daughter particles, which are easier to resolve.

In Fig. 8, we show the matching accuracy of QAOA (solid, yellow), ma-QAOA (dashed, orange), FALQON (dotted, red) and hemisphere (black, dot-dashed) for parton-level events for using Eq. (1) only (left) and using full Hamiltonian (Eq. (1) and Eq. (5)), $H = H_0 + \lambda H_1$. The matching accuracy represents the efficiency of each method, indicating the fraction of events that are successfully resolved by each approach.

The boostness is illustrated by $m_{t\bar{t}}/(2m_t)$, where $m_{t\bar{t}}$ is the invariant mass of the two top quarks and m_t is the top quark mass. The shaded region represents matching accuracy for a theoretical algorithm that chose the minimum eigenstate for every event, indicating the effectiveness of the Hamiltonian. Any quantum algorithms that we consider can not lead to results that is better than the shaded region. The region around $m_{t\bar{t}}/(2m_t) \sim 1$ represents the threshold production, where the decay products of the top quarks are approximately isotropically distributed. In this case, the combinatorial problem is harder to resolve and the matching accuracy is low for all methods. Especially, the hemisphere method is significantly affected by the boostness, while quantum algorithms with the leading Hamiltonian (the mass square difference in Eq. (1) is less sensitive, as shown in the left panel.

However, when the two top quarks are very boosted ($m_{t\bar{t}}/(2m_t) \geq 2.5$), the hemisphere method outperforms all other methods. Although overall accuracy is still much higher with quantum algorithms. To further im-

prove the performance of quantum algorithms, we have considered the second term (Eq. (5)) in the Hamiltonian. Indeed, the revised Hamiltonian $H = H_0 + \lambda H_1$ leads to the substantial enhancement in the region with $m_{t\bar{t}}/(2m_t) \geq 1.5$. While the performance near the threshold is quite suppressed, the total efficiency of the revised Hamiltonian is much better than the case without it. The performance near the threshold is still better than that for the hemisphere method. We note that since the hemisphere method is independent of the cost function or Hamiltonian, the two curves in the left and right are identical.

One important question is how to choose the depth of quantum circuits. Fig. 9 shows the success rates of QAOA (blue), ma-QAOA (red) and XQAOA (purple) as a function of the number of iterations (depth) for parton-level events using the full Hamiltonian in Eq. (6). The solid curves labeled as “Minimum” represent the success rate of the algorithm in finding the correct ground state, while the dotted curves labeled as “Correct” show the matching accuracy (efficiency) in resolving the combinatorial problem. As expected, ma-QAOA and XQAOA converge to $\sim 80\%$ matching accuracy rather quickly around $p = \mathcal{O}(2)$, while the QAOA results fluctuate significantly and therefore require many more iterations.

Finally we compare quantum algorithms against machine learning (ML) methods. We chose to use SPANet [4, 5], which is a symmetry-preserving attention network reflecting the problem’s natural invariance to efficiently find assignments without evaluating all permutations. Refs. [4, 5] showed that this general approach is applicable to arbitrarily complex configurations and significantly outperforms current methods. Fig. 10 shows the

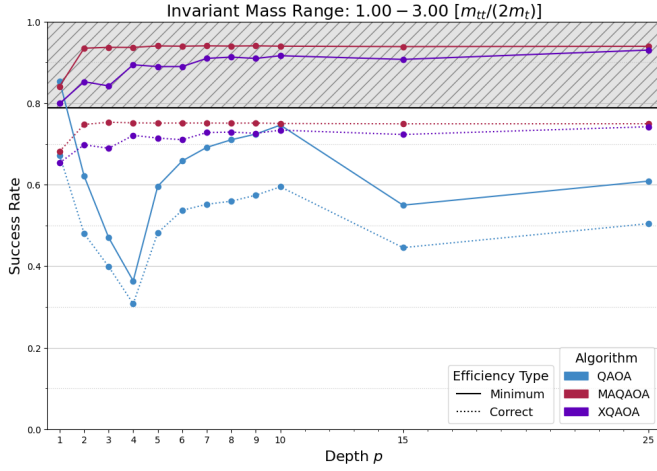


FIG. 9. The success rate of QAOA (blue), ma-QAOA (red), and XQAOA (purple) as a function of the number of iterations (depth, p) for parton-level events using the full Hamiltonian is shown. The solid curves represent how well the Hamiltonian finds the ground state correctly, while the dotted curves represent how well the quantum algorithm resolves the combinatorial problem.

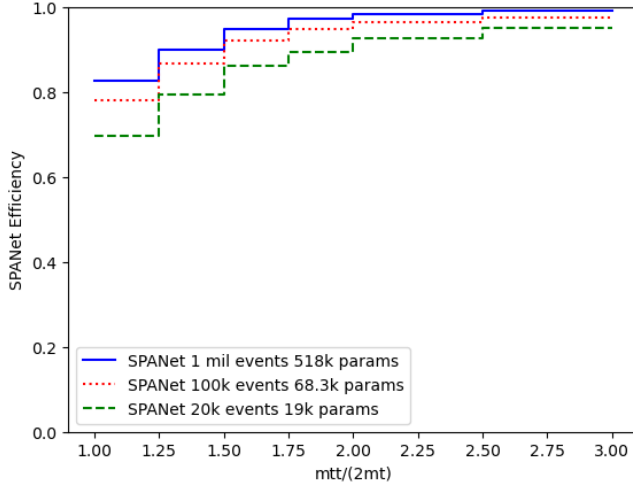


FIG. 10. Efficiency plot for parton-level events using SPANet [4, 5] for several different number of training events and number of the network parameters. The corresponding overall efficiencies are 90.7% (blue, solid), 87.4% (red, dotted) and 80.7% (green, dashed), respectively.

efficiency for parton-level events using SPANet for several different number of training events (n_{train}) and number of learnable parameters (n_{params}), blue for $(n_{\text{train}}, n_{\text{params}}) = (1 \text{ mil}, 518\text{k})$, red for $(n_{\text{train}}, n_{\text{params}}) = (100\text{k}, 68.3\text{k})$ and green for $(n_{\text{train}}, n_{\text{params}}) = (20\text{k}, 19\text{k})$. The corresponding overall efficiencies are 90.7% (blue, solid), 87.4% (red, dotted) and 80.7% (green, dashed), respectively. These results are obtained with the default settings in SPANet with AdamW optimizer [79].

There are several notable differences between quan-

tum algorithms and ML methods. First, quantum algorithms are independent of the particle masses, while the top mass information is indirectly learned in ML methods. If the top mass changes, ML needs new training. Second, quantum algorithms do not require the training step at all and the Hamiltonian is computed on an event-by-event basis, while ML methods learn properties of all training samples. However, QAOA and its variants require an optimization process, while FALQON does not. Third, SPANet is a supervised learning algorithm, which assumes the event-topology (2-step 2-body in this study). On the other hand, the quantum algorithms advertised in this paper do not require any training nor event topology. Finally, SPANet is the state of art ML method for resolving the combinatorial problem in the multi-jet final state [4, 5], and quantum algorithms that we have investigated already give comparable results. Considering the current era is only the beginning of quantum algorithms, we anticipate substantial improvement with new quantum algorithms in near future.

We summarize some of the important parameters in Table I for the various methods we investigated in resolving the combinatorial ambiguities in the fully hadronic production of top pairs. The corresponding accuracies or efficiencies for both parton-level and smeared events are also presented. (see Appendix C for description of smeared events.) The QAOA, ma-QAOA and FALQON all have the same number of gates. For q qubits, each layer contains $\binom{q}{2} R_{ZZ}$ gates and $q R_X$ gates, and each R_{ZZ} gate includes 2 CNOT gates and 1 R_Z gate, which leads to $2\binom{q}{2} \text{CNOT} + \binom{q}{2} R_Z + q R_X$ gates for each layer. Therefore there are $2p\binom{q}{2}$ CNOT gates (n_{CNOT}), $p\binom{q}{2} R_Z$ gates (n_{R_Z}) and $pq R_X$ gates (n_{R_X}). For $p = 8$, the circuit contains 240 CNOT gates, 120 R_Z gates and 48 R_X gates. FALQON with depth $p = 250$ uses 7500 CNOT gates, 3750 R_Z gates and 1500 R_X . The numbers of parameters ($n_{\text{parameters}}$) is $2p = 16$ for for QAOA and $p(q + \binom{q}{2}) = 168$ for ma-QAOA. FALQON uses only two free parameters Δt and β_1 . ML methods such as SPANet needs the training procedure, which requires the sufficient number of training samples (n_{train}) and a large number of parameters ($n_{\text{parameters}}$). We note that $n_{\text{parameters}}$ represents two distinct concepts: the count of learnable parameters for SPANet and the number of adjustable parameters for quantum algorithms, respectively.

When discussing the performance of a quantum algorithm, the number of CNOT gates is often counted because CNOT gates are a key building block for creating entanglement between qubits, which is a crucial aspect of many quantum algorithms, and therefore, the number of CNOT gates directly impacts the complexity and execution time of the algorithm on a quantum computer [80, 81].

Methods	matching accuracy (efficiency)		n_{train}	$n_{\text{parameters}}$	depth (p)	n_{CNOT}	n_{Rz}	n_{Rx}
	parton-level	smear events						
Hemisphere	50%	48%	N/A					
QAOA	55%	53%	N/A	16	8	240	120	48
ma-QAOA	75%	73%		168				
FALQON	72%	69%		2	250	7,500	3,750	1,500
SPANet	91%	70%	5×10^5	10^6	N/A			
	81%	62%	2×10^4	1.9×10^3				

TABLE I. Summary of the performance of various methods and the corresponding parameters.

VI. SUMMARY AND OUTLOOK

Combinatorial problems have become a major challenge in particle physics experiments. Unlike the simpler environment of lepton colliders, hadron colliders involve numerous jets - some from heavy particle decays and others from initial state radiation - making event reconstruction complex. Finite detector resolution and the inability to distinguish quarks from anti-quarks add to this difficulty. Solving the combinatorial challenge of associating jets with specific particle decays improves the precision of particle measurements and advances the discovery of new physics via better identification of event topology and determination of masses and spins [2]. Several ideas have been proposed including kinematic methods and ML approaches. In this paper, we have proposed the use of quantum algorithms and compared them against existing methods, taking the fully hadronic channel of the top quark production at the LHC as a concrete example. We have investigated the performance of two types of quantum algorithms: variational quantum algorithms (QAOA and its variants) and a feedback based algorithm (FALQON). We have used 6 qubits corresponding to 6 particles in the final state. Our results showed that the efficiency for selecting the correct pairing is greatly improved by utilizing quantum algorithms over conventional kinematic methods. Performance of quantum algorithms is comparable to ML methods, especially with the smeared events. These quantum algorithms are scalable and can be easily generalizable to n particles [82–85].

Hybrid quantum-classical algorithms such as VQAs are well-suited for current noisy quantum devices, leveraging a hybrid approach that combines quantum circuits with classical optimization to solve complex problems [40–42]. Their flexibility and resource efficiency make them ideal for various tasks in optimization and machine learning problems, while also offering some resilience to noise. However, they face challenges such as the potential inefficiency of classical optimizers, difficulty in selecting the

right ansatz, and the risk of barren plateaus, where optimization stagnates. Additionally, while VQAs are more noise-tolerant than some algorithms, scalability remains limited due to noise and classical bottlenecks [86]. On the other hand, feedback-based quantum algorithms offer real-time adaptability, allowing quantum operations to be adjusted based on intermediate measurements, which helps mitigate noise and improve precision, especially in quantum sensing and control. They are crucial for certain quantum error correction techniques and can optimize the use of available resources by reducing the need for deep circuits. However, frequent measurements risk collapsing quantum states, increasing complexity and overhead due to the need for fast classical processing. In some cases, feedback can amplify noise if not properly designed, and the approach may not be broadly applicable across all quantum algorithms [11].

In general, kinematic methods and quantum algorithms do not require a training process, whereas ML methods heavily depend on training a network with numerous events. VQAs involve parameter optimization using classical optimizers, while feedback-based algorithms do not. It is important to note that each method has its own strengths and weaknesses. The performance of different methods can vary depending on the underlying event topology and the study point, meaning no single method is consistently superior. Therefore it is prudent to keep a broad range of methods available in the analysis toolbox.

The interplay between these methods highlights the tension between optimality and generalizability. While the straightforward kinematic methods are robust and universally applicable (model-independent), their performance is not the best. In contrast, the ML methods offer greater sensitivity and improved physics performance, but they are not easily generalizable to other signal processes (need to train again). Quantum algorithms provide an alternative solution to the combinatorial problems but they have their own challenges such as

- the effect of quantum noise (appendix B),
- detector effects (appendix C), and
- the performance of quantum algorithms for different processes (appendix D).

In the Appendix, we will make short comments on some of these points as well as quantum algorithms based on a non-adiabatic path (appendix E). However to make quantum algorithms more practical, a more in-depth investigation is necessary.

Acknowledgements: We thank Konstantin Matchev, Sergei Gleyzer, Andrea Delgado and Talal Chowdhury for useful discussion, and Ahamed Hammad for introducing us FALQON algorithm. KK is supported in parts by US DOE DE-SC0024407. JS is supported by US DOE AI-HEP grant DE-SC0024673. JS and CD is supported in part by College of Liberal Arts and Sciences Research Fund at the University of Kansas. TK is supported in part by the National Science Foundation (NSF) under Grant CNS2212565, Grant CNS2225577, and Grant CNS1955561, and the Office of Naval Research (ONR) under Grant N000142112472. MP was supported by the National Research Foundation of Korea (NRF) under grant NRF-2021R1A2C4002551 during the early stages of this work. MP and KK would like to thank the Aspen Center for Physics and the organizers of Summer 2024 workshop, “Fundamental Physics in the Era of Big Data and Machine Learning” (supported by National Science Foundation grant PHY-2210452) for hospitality during the completion of this manuscript.

Appendix A: Quantum circuits

The schematic QAOA diagram of depth p for n qubits is shown in Fig. 11, where $U(\beta, H_M)$ and $U(\gamma_i, H_P)$ are shown in Fig. 12 and Fig. 13, respectively. H is the Hadamard gate, R_X and R_Z are Pauli rotations of X and Z . In the cost layer as shown in Fig. 13, each vertical bar represents the $R_{ZZ}(\gamma_i)$ gate between the two qubits. As shown decomposed into common basis gates in the inlay. The gate applied to qubits q_s and q_t is defined by $R_{ZZ}(\gamma_i) \equiv \exp[-Z_s Z_t \gamma_i]$ where Z_s (Z_t) is the Pauli Z gate acting on qubit q_s (q_t), which in practice are decomposed into CNOT gates and single-qubit Pauli Z rotation. Fig. 14 shows the mixer layer in the i -th layer of ma-QAOA for n qubits, which is similar to the mixer layer of QAOA in Fig. 12. However the Mixer layer of ma-QAOA has a vector β_i of parameters such that each qubit receives its own rotation that the optimizer can freely vary.

The basic idea of FALQON is summarized in Fig. 15 (taken from Ref. [73]). The procedure for implementing FALQON begins by setting the initial condition $\beta_1 = 0$, as shown in Fig. 15(a). The qubits are first prepared

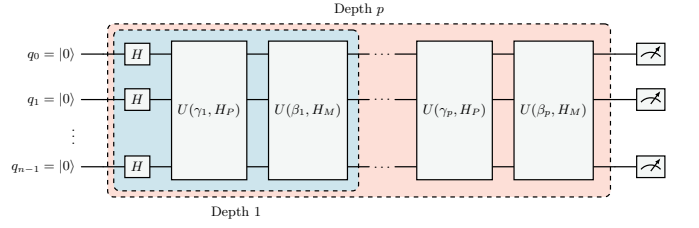


FIG. 11. QAOA of depth p for n qubits.

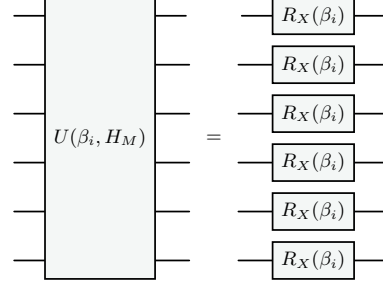


FIG. 12. The i -th mixer layer of QAOA for $n = 6$ qubits.

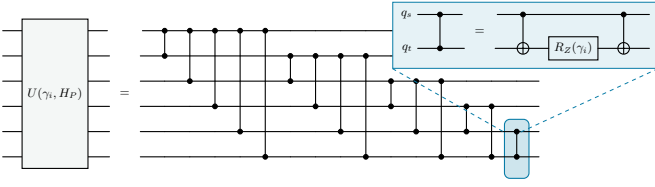
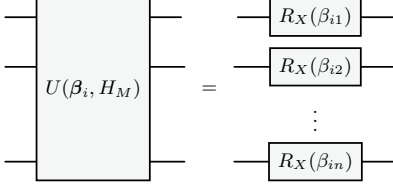
in the state $|\psi_0\rangle$, followed by applying a single FALQON layer to generate $|\psi_1\rangle = U_M(\beta_1)U_P|\psi_0\rangle$. After this, the qubits are measured to estimate A_1 , which is then used to set $\beta_2 = -A_1$. In subsequent steps, for $k = 2, \dots, p$, the process is repeated as described in Fig. 15(b): the qubits are initialized in $|\psi_0\rangle$, and k layers are applied to produce $|\psi_k\rangle = U_M(\beta_k)U_P \dots U_M(\beta_1)U_P|\psi_0\rangle$. The qubits are then measured to estimate A_k , and the result is used to update β_{k+1} . This iterative process ensures that $\langle H_P \rangle$ decreases with each layer, as shown in Fig. 15(c): $\langle \psi_1 | H_P | \psi_1 \rangle \geq \langle \psi_2 | H_P | \psi_2 \rangle \geq \dots \geq \langle \psi_p | H_P | \psi_p \rangle$. This layer-by-layer reduction improves the quality of the solution to the combinatorial optimization problem as the circuit depth increases. The procedure can be halted when $\langle H_P \rangle$ converges or when a predefined number of layers p is reached. Finally, Z -basis measurements on $|\psi_p\rangle$ can be used to identify the best candidate solution to the combinatorial optimization problem by repeatedly sampling from the bit string distribution defined by $|\psi_p\rangle$ and selecting the outcome corresponding to the optimal solution.

Appendix B: Effects of quantum noise

Quantum noise can be modeled as a set of operators $\{E_k\}$ that obey the completeness relation,

$$\sum_k E_k^\dagger E_k = I, \quad (\text{B1})$$

and act on the density matrix of the quantum system as $\mathcal{E}(\rho) = \sum_k E_k \rho E_k^\dagger$. In practice, for a single qubit, these operators can often be written as a linear combination of

FIG. 13. The i -th cost or problem layer of QAOA.FIG. 14. The i -th mixer layer of ma-QAOA for n qubits.

Pauli matrices,

$$E_k = \alpha_k I + \sum_{i=1}^3 \beta_{ki} \sigma_i. \quad (\text{B2})$$

Using this form, we can define a few commonly used noise channels. The *bit flip* channel is given by

$$E_0 = \sqrt{1-p}I, \quad E_1 = \sqrt{p}X, \quad (\text{B3})$$

wherein, with probability p , a bit flip occurs, i.e. an X gate. Likewise, a *phase flip* channel is given by

$$E_0 = \sqrt{1-p}I, \quad E_1 = \sqrt{p}Z. \quad (\text{B4})$$

The *depolarizing channel* represents a uniform contraction of the Bloch sphere. Physically, there is a probability p that the qubit is depolarized. It is given by

$$\mathcal{E}(\rho) = \frac{p}{2}I + (1-p)\rho \quad (\text{B5})$$

or, the operator representation,

$$E_0 = \sqrt{1-p}I, \quad E_i = \sqrt{p/3}P_i \quad (\text{B6})$$

where $P_1 = X$, $P_2 = Y$, and $P_3 = Z$. Lastly, *amplitude damping* encodes potential energy dissipation of the qubit, say the spontaneous emission of a photon. Its operators are

$$E_0 = \begin{pmatrix} 1 & 0 \\ 0 & \sqrt{1-\gamma} \end{pmatrix}, \quad E_1 = \begin{pmatrix} 0 & \sqrt{\gamma} \\ 0 & 0 \end{pmatrix} \quad (\text{B7})$$

where $\gamma \in [0, 1]$ is the amplitude damping probability, e.g. a representation of the probability to emit a photon.

There are additional, commonly used, operator representations of noise, such as generalized amplitude damping and phase damping, which represent additional modes of quantum information loss, but they are not discussed here. More information can be found in [87].

The error rates are different, depending on quantum computing architecture. Nevertheless, the two-qubit gate error rate is about 1% for most current quantum computers and some of them are already close to $\sim 0.1\%$ [88], which we take to be our benchmark points. Fig. 16 shows the efficiency of ma-QAOA with bitflip noise on every gate for 0.1% (dashed) and 1% error rate (dotted). The solid curve represent the ideal case (no noise). Results are obtained for depths of $p = 3$. We anticipate that future improvements will significantly reduce the error rate, potentially minimizing the impact of quantum noise. However, exploring error correction in this combinatorial optimization problem remains valuable.

Appendix C: Detector effects

To simulate detector effects, we follow the parametrization used in ATLAS detector performances report for the HL-LHC [89]. The energy resolution is parameterized by three terms; noise (N), stochastic (S), and constant (C) terms

$$\frac{\sigma}{E} = \sqrt{\left(\frac{N}{E}\right)^2 + \left(\frac{S}{\sqrt{E}}\right)^2 + C^2}, \quad (\text{C1})$$

where in our analysis we use $N = 5.3$, $S = 0.74$ and $C = 0.05$ for jets, and the energy E is in GeV. We smear particle momenta of parton-level events following the above parametrization and refer to this dataset as ‘‘Smeared events’’. Basic cuts of $p_T > 25$ GeV, rapidity $|\eta| < 2.5$ and $\Delta R(j, j) > 0.4$ are applied to the smeared particles. Fig. 17 shows the matching accuracy of QAOA (solid), ma-QAOA (dashed), FALQON (dotted) and hemisphere (dot-dashed) for parton-level events (left) and smeared events (right) using both Eq. (1) and Eq. (5) for the full Hamiltonian, $H = H_0 + \lambda H_1$. The performance degrades slightly but remains very similar, showing the robustness of the quantum algorithms. Table I presents the matching accuracy for various methods across both parton-level and smeared events, showing that quantum algorithms exhibit only slight changes, while ML methods undergo a noticeable degradation. Spanet is trained

While these results are quite promising, a more thorough investigation is needed including ISR and parton shower / hadronization and more realistic detector simulation.

Appendix D: Different processes with the same final state

In this section, we apply the QAOA algorithm to tW with 5 jets and QCD production with 6 jets. Fig. 18 shows the reconstructed masses (left) and jet-assignment (right) with parton-level events using QAOA with depth $p = 8$ for tW production (top) and multi-jet

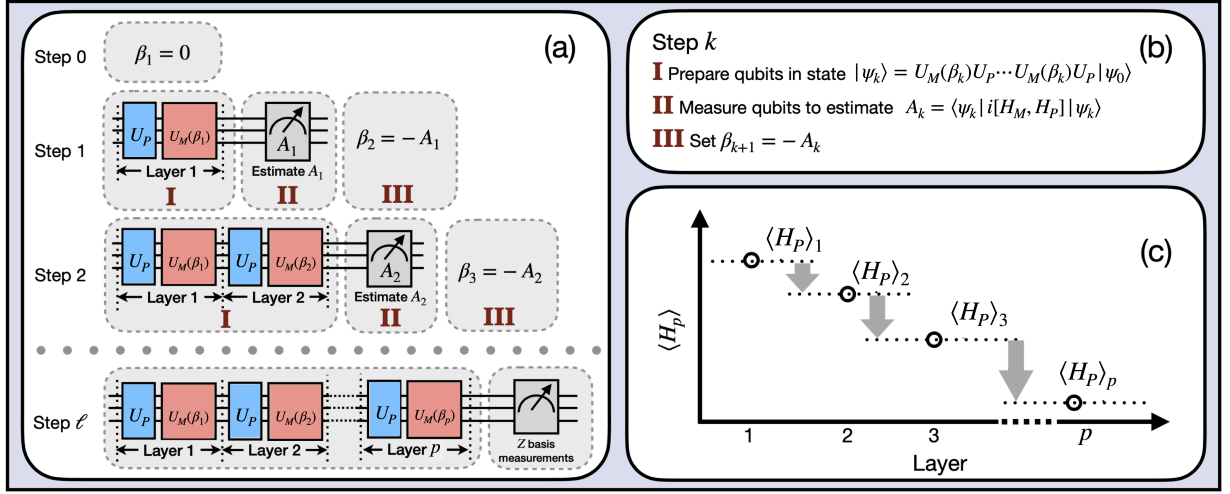


FIG. 15. Illustration of the FALQON algorithm. Taken from Ref. [73].

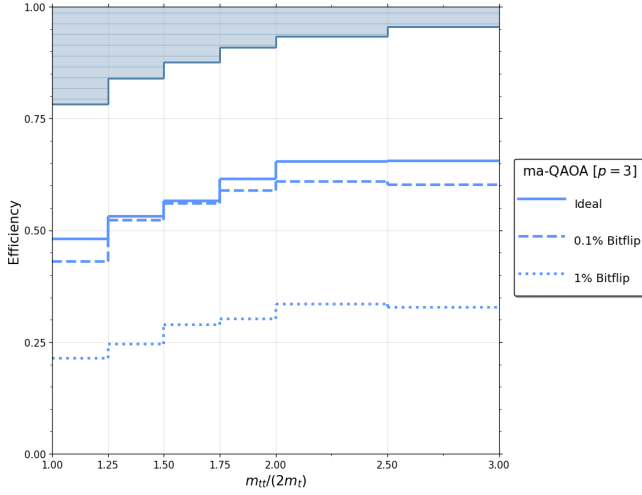


FIG. 16. Efficiency plot for ma-QAOA with bitflip noise on every gate for the ideal case (solid), 0.1% chance (dashed) and 1% chance (dotted). Shown are for depths of $p = 3$.

production (bottom). The ground state is found for the full Hamiltonian. As expected, the top panel shows a large concentration near the correct masses $(m_t, m_W) = (173, 80)$ GeV with the correct jet assignment for top and W boson, even if the mass information is not used in QAOA (quantum algorithms in general). The overall efficiency for tW is 22%. Similarly, since the multi-jet production does not have a specific mass scale, the bottom panel shows that most events are populated near zero mass with random jet assignment. It is important to note that the same Hamiltonians in Eqs. (4-6) lead to these results. We used 12k tW and 3k 6 jet events.

Appendix E: ADAPT-QAOA

As an example of quantum algorithms based on a non-adiabatic path, we consider the Adaptive Derivative Assembled Problem Tailored QAOA [90] (ADAPT-QAOA). In this algorithm, the choice of the mixer Hamiltonian is not fixed but instead is drawn from a pool of potential Hamiltonians layer by layer. The k -th layer will have $H_M = A_k$ where A_k one of single-qubit mixers (E1) or multi-qubit mixers (E2):

$$\text{Single-qubit mixers} \begin{cases} X_i & - \text{ An } X \text{ gate on the } i\text{th qubit} \\ Y_i & - \text{ A } Y \text{ gate on the } i\text{th qubit} \\ \sum_{i=1}^n X_i & - \text{ An } X \text{ gate on every qubit, i.e. QAOA} \\ \sum_{i=1}^n Y_i & - \text{ A } Y \text{ gate on every qubit} \end{cases} \quad (\text{E1})$$

$$\text{Multi-qubit mixers} \begin{cases} X_i X_j & - \text{ } X \text{ gates on the } i\text{th and } j\text{th qubits, respectively} \\ X_i Y_j & - \text{ } X \text{ and } Y \text{ gates on the } i\text{th and } j\text{th qubits, respectively} \\ X_i Z_j & - \text{ } X \text{ and } Z \text{ gates on the } i\text{th and } j\text{th qubits, respectively} \\ Y_i Z_j & - \text{ } Y \text{ and } Z \text{ gates on the } i\text{th and } j\text{th qubits, respectively} \\ Y_i Y_j & - \text{ } Y \text{ gates on the } i\text{th and } j\text{th qubits, respectively} \\ Z_i Z_j & - \text{ } Z \text{ gates on the } i\text{th and } j\text{th qubits, respectively} \end{cases} \quad (\text{E2})$$

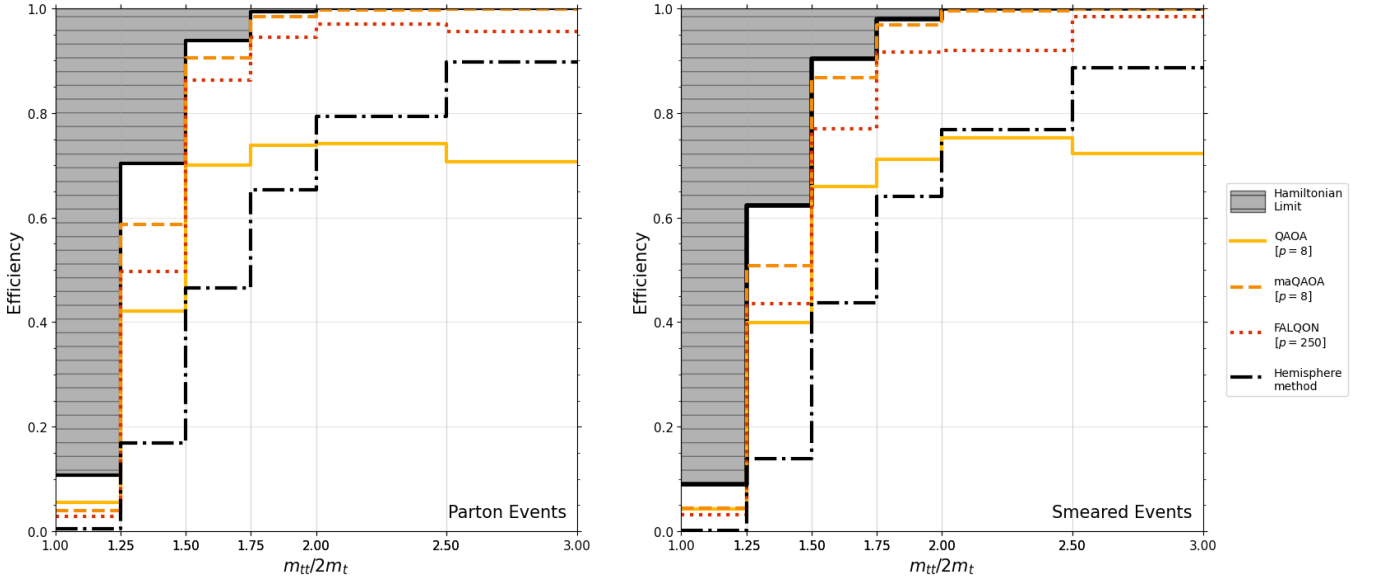


FIG. 17. The matching accuracy (efficiency) of QAOA (solid), ma-QAOA (dashed), FALQON (dotted) and hemisphere (dot-dashed) for parton-level events (left) and smeared events (right) with the Hamiltonian, $H = H_0 + \lambda H_1$.

Namely, the two QAOA-like mixers (the third and fourth above) and all length one and two Pauli strings. As such, ADAPT-QAOA shares similarities with FALQON as the circuit is iteratively built. For layer k ,

we aim to find the mixer that maximizes the energy gradient. That is, if \mathcal{A} is the mixer pool, then $\forall A_j \in \mathcal{A}$, we calculate

$$\Delta E_k^j \equiv \frac{\partial}{\partial \beta_k} \langle \psi_k | H_P | \psi_k \rangle \Big|_{\beta_k=0} = \frac{\partial}{\partial \beta_k} \langle \psi_{k-1} | e^{i\gamma_k H_P} e^{i\beta_k A_j} H_P e^{-i\beta_k A_j} e^{-i\gamma_k H_P} | \psi_{k-1} \rangle \Big|_{\beta_k=0} \quad (\text{E3})$$

$$= \langle \psi_{k-1} | e^{i\gamma_k H_P} e^{i\beta_k A_j} (iA_j H_P - iH_P A_j) e^{-i\beta_k A_j} e^{-i\gamma_k H_P} | \psi_{k-1} \rangle \Big|_{\beta_k=0} \quad (\text{E4})$$

$$= -i \langle \psi_{k-1} | e^{i\gamma_k H_P} [H_P, A_j] e^{-i\gamma_k H_P} | \psi_{k-1} \rangle \quad (\text{E5})$$

and choose $A_k = \underset{A_j \in \mathcal{A}}{\text{argmax}} \Delta E_k^j$. Since we don't know γ_k a priori, we set it to some predefined value γ_0 . Once the mixer for the k th layer, A_k , has been chosen, the parameter of the k th layer is optimized as with normal QAOA. This optimization procedure is then repeated layer by layer while keeping all previous layers fixed. The algorithm can be stopped when a specific circuit depth has been reached or ΔE_k^j is below some threshold. The improvement provided by ADAPT-QAOA comes taking a shortcut non-adiabatic path[91]. One downside to this method is the large mixer pool could potentially lead

to a lot of measurements. We attempted to implement this algorithm but ADAPT-QAOA did not improve the matching efficiency.

There are a few other studies on manipulating the adiabatic path of QAOA-type algorithms [92, 93]. Other physics-inspired QAOA variants include Mean-Field Approximate Optimization Algorithm [94], Improving Quantum Approximate Optimization by Noise-Directed Adaptive Remapping [95], ADAPT-QAOA with a classically inspired initial state[96] and Dynamic-ADAPT-QAOA with shallow and noise-resilient circuits [97]

[1] Shoji Asai *et al.* (P5), “Exploring the Quantum Universe: Pathways to Innovation and Discovery in Parti-

cle Physics,” (2023), 10.2172/2368847, arXiv:2407.19176

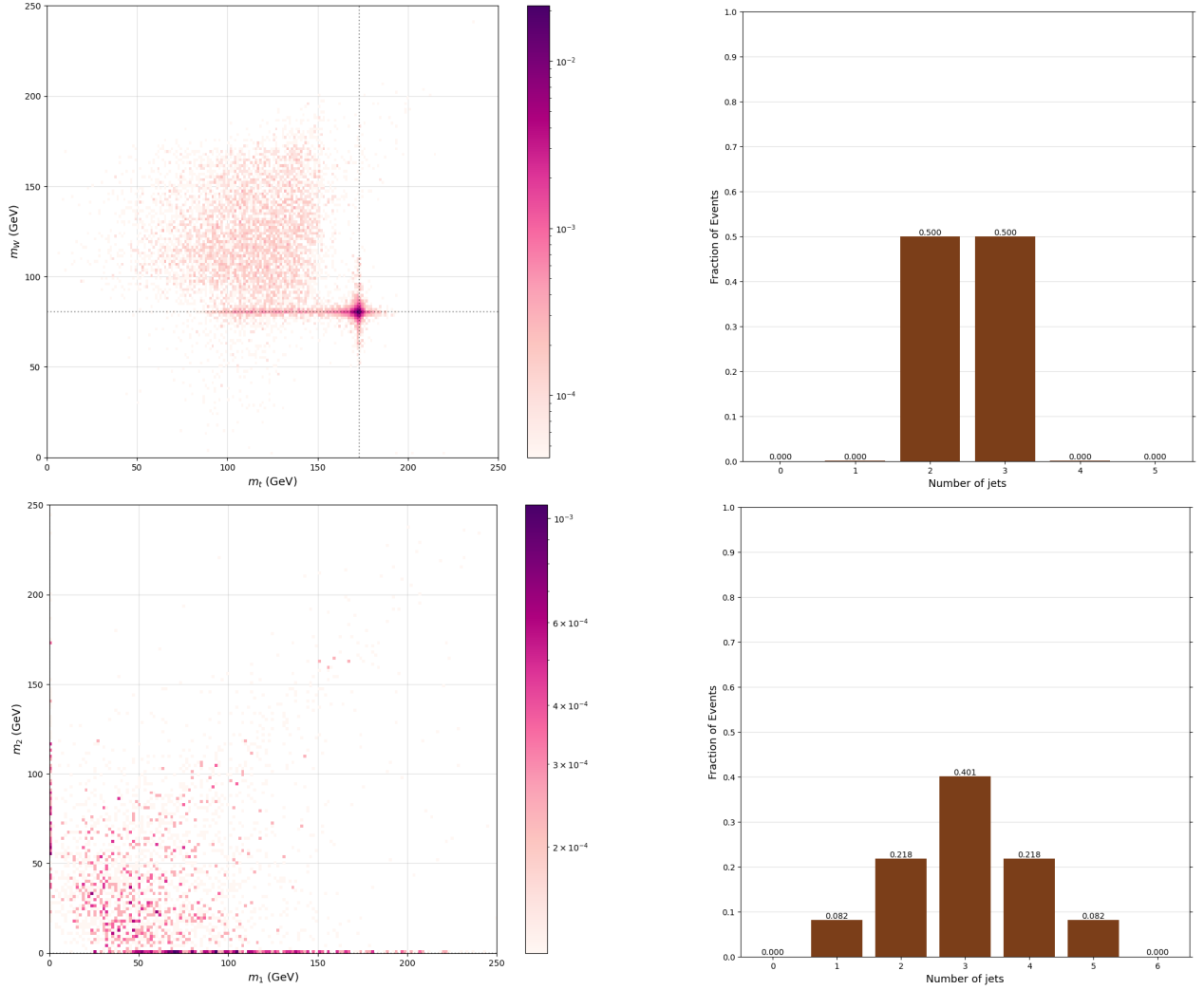


FIG. 18. The same as Fig. 5 but for tW production (top) and multi-jet production (bottom). The reconstructed masses (left) and jet-assignment (right) for parton-level events using ma-QAOA with depth $p = 8$. The ground state is found for the full Hamiltonian. The overall efficiency for tW is 22%. Results using FALQON (not shown) are similar to those using ma-QAOA.

- [1] [hep-ex].
- [2] Roberto Franceschini, Doojin Kim, Kyoungchul Kong, Konstantin T. Matchev, Myeonghun Park, and Prasanthy Shyamsundar, “Kinematic variables and feature engineering for particle phenomenology,” *Rev. Mod. Phys.* **95**, 045004 (2023), arXiv:2206.13431 [hep-ph].
- [3] Alan J. Barr and Christopher G. Lester, “A Review of the Mass Measurement Techniques proposed for the Large Hadron Collider,” *J. Phys. G* **37**, 123001 (2010), arXiv:1004.2732 [hep-ph].
- [4] Alexander Shmakov, Michael James Fenton, Ta-Wei Ho, Shih-Chieh Hsu, Daniel Whiteson, and Pierre Baldi, “SPANet: Generalized permutationless set assignment for particle physics using symmetry preserving attention,” *SciPost Phys.* **12**, 178 (2022), arXiv:2106.03898 [hep-ex].
- [5] Michael James Fenton, Alexander Shmakov, Ta-Wei Ho, Shih-Chieh Hsu, Daniel Whiteson, and Pierre Baldi, “Permutationless many-jet event reconstruction with symmetry preserving attention networks,” *Phys. Rev. D* **105**, 112008 (2022), arXiv:2010.09206 [hep-ex].
- [6] Jason Sang Hun Lee, Inkyu Park, Ian James Watson, and Seungjin Yang, “Zero-permutation jet-parton assignment using a self-attention network,” *J. Korean Phys. Soc.* **84**, 427–438 (2024), arXiv:2012.03542 [hep-ex].
- [7] Haider Alhazmi, Zhongtian Dong, Li Huang, Jeong Han Kim, Kyoungchul Kong, and David Shih, “Resolving combinatorial ambiguities in dilepton tt^- event topologies with neural networks,” *Phys. Rev. D* **105**, 115011 (2022), arXiv:2202.05849 [hep-ph].
- [8] Edward Farhi, Jeffrey Goldstone, and Sam Gutmann, “A Quantum Approximate Optimization Algorithm,” (2014), arXiv:1411.4028 [quant-ph].
- [9] Kostas Blekos, Dean Brand, Andrea Ceschini, Chiao-Hui Chou, Rui-Hao Li, Komal Pandya, and Alessandro Summer, “A review on Quantum Approximate Optimization Algorithm and its variants,” *Phys. Rept.* **1068**, 1–66 (2024), arXiv:2306.09198 [quant-ph].
- [10] Seongmin Kim, Tengfei Luo, Eungkyu Lee, and In-Saeng Suh, “Distributed Quantum Approximate Optimization

- Algorithm on Integrated High-Performance Computing and Quantum Computing Systems for Large-Scale Optimization,” (2024), [arXiv:2407.20212 \[cs.DC\]](#).
- [11] Alicia B. Magann, Kenneth M. Rudinger, Matthew D. Grace, and Mohan Sarovar, “Feedback-Based Quantum Optimization,” *Phys. Rev. Lett.* **129**, 250502 (2022), [arXiv:2103.08619 \[quant-ph\]](#).
- [12] Minh Kim, Pyungwon Ko, Jae-hyeon Park, and Myeonghun Park, “Leveraging Quantum Annealer to identify an Event-topology at High Energy Colliders,” (2021), [arXiv:2111.07806 \[hep-ph\]](#).
- [13] Shigeki Matsumoto, Mihoko M. Nojiri, and Daisuke Nomura, “Hunting for the Top Partner in the Littlest Higgs Model with T-parity at the CERN LHC,” *Phys. Rev. D* **75**, 055006 (2007), [arXiv:hep-ph/0612249](#).
- [14] G. L. Bayatian *et al.* (CMS), “CMS technical design report, volume II: Physics performance,” *J. Phys. G* **34**, 995–1579 (2007).
- [15] Andrew J. Daley, Immanuel Bloch, C. Kokail, Stuart Flannigan, N Pearson, Matthias Troyer, and Peter Zoller, “Practical quantum advantage in quantum simulation,” *Nature* **607**, 667 – 676 (2022).
- [16] Nils Herrmann, Daanish Arya, Marcus W. Doherty, Angus Mingare, Jason C. Pillay, Florian Preis, and Stefan Prestel, “Quantum utility – definition and assessment of a practical quantum advantage,” (2023), [arXiv:2303.02138 \[quant-ph\]](#).
- [17] Amira Abbas *et al.*, “Quantum Optimization: Potential, Challenges, and the Path Forward,” (2023), [arXiv:2312.02279 \[quant-ph\]](#).
- [18] Alberto Di Meglio *et al.*, “Quantum Computing for High-Energy Physics: State of the Art and Challenges,” *PRX Quantum* **5**, 037001 (2024), [arXiv:2307.03236 \[quant-ph\]](#).
- [19] Christian W. Bauer, Wibe A. de Jong, Benjamin Nachman, and Davide Provasoli, “Quantum Algorithm for High Energy Physics Simulations,” *Phys. Rev. Lett.* **126**, 062001 (2021), [arXiv:1904.03196 \[hep-ph\]](#).
- [20] Christian W. Bauer, Marat Freytsis, and Benjamin Nachman, “Simulating Collider Physics on Quantum Computers Using Effective Field Theories,” *Phys. Rev. Lett.* **127**, 212001 (2021), [arXiv:2102.05044 \[hep-ph\]](#).
- [21] Khadeejah Bepari, Sarah Malik, Michael Spannowsky, and Simon Williams, “Towards a quantum computing algorithm for helicity amplitudes and parton showers,” *Physical Review D* **103** (2021), [10.1103/physrevd.103.076020](#).
- [22] Gösta Gustafson, Stefan Prestel, Michael Spannowsky, and Simon Williams, “Collider events on a quantum computer,” *JHEP* **11**, 035 (2022), [arXiv:2207.10694 \[hep-ph\]](#).
- [23] Hideki Okawa, Xian-Zhe Tao, Qing-Guo Zeng, and Man-Hong Yung, “Quantum-annealing-inspired algorithms for multijet clustering,” (2024), [arXiv:2410.14233 \[quant-ph\]](#).
- [24] Yongfeng Zhu, Weifeng Zhuang, Chen Qian, Yunheng Ma, Dong E. Liu, Manqi Ruan, and Chen Zhou, “A Novel Quantum Realization of Jet Clustering in High-Energy Physics Experiments,” (2024), [arXiv:2407.09056 \[quant-ph\]](#).
- [25] Jorge J. Martínez de Lejarza, Leandro Cieri, and Germán Rodrigo, “Quantum clustering and jet reconstruction at the LHC,” *Phys. Rev. D* **106**, 036021 (2022), [arXiv:2204.06496 \[hep-ph\]](#).
- [26] Diogo Pires, Pedrame Bargassa, João Seixas, and Yasser Omar, “A Digital Quantum Algorithm for Jet Clustering in High-Energy Physics,” (2021), [arXiv:2101.05618 \[physics.data-an\]](#).
- [27] Diogo Pires, Yasser Omar, and João Seixas, “Adiabatic quantum algorithm for multijet clustering in high energy physics,” *Phys. Lett. B* **843**, 138000 (2023), [arXiv:2012.14514 \[hep-ex\]](#).
- [28] Annie Y. Wei, Preksha Naik, Aram W. Harrow, and Jesse Thaler, “Quantum Algorithms for Jet Clustering,” *Phys. Rev. D* **101**, 094015 (2020), [arXiv:1908.08949 \[hep-ph\]](#).
- [29] Andrea Delgado and Jesse Thaler, “Quantum annealing for jet clustering with thrust,” *Phys. Rev. D* **106**, 094016 (2022), [arXiv:2205.02814 \[quant-ph\]](#).
- [30] Cenk Tüysüz, Federico Carminati, Bilge Demirköz, Daniel Dobos, Fabio Fracas, Kristiane Novotny, Karolos Potamianos, Sofia Vallecorsa, and Jean-Roch Vlimant, “Particle Track Reconstruction with Quantum Algorithms,” *EPJ Web Conf.* **245**, 09013 (2020), [arXiv:2003.08126 \[quant-ph\]](#).
- [31] Lena Funcke, Tobias Hartung, Karl Jansen, and Stefan Kühn, “Review on quantum computing for lattice field theory,” in *Proceedings of The 39th International Symposium on Lattice Field Theory — PoS(LATTICE2022)* (Sissa Medialab, 2023).
- [32] Ji-Chong Yang, Shuai Zhang, and Chong-Xing Yue, “A novel quantum machine learning classifier to search for new physics,” (2024), [arXiv:2410.18847 \[hep-ph\]](#).
- [33] J. Ignacio Cirac and Peter Zoller, “Goals and opportunities in quantum simulation,” *Nature Physics* **8**, 264–266 (2012).
- [34] I. M. Georgescu, S. Ashhab, and Franco Nori, “Quantum simulation,” *Reviews of Modern Physics* **86**, 153–185 (2014).
- [35] Andrea Delgado *et al.*, “Quantum Computing for Data Analysis in High-Energy Physics,” in *Snowmass 2021* (2022) [arXiv:2203.08805 \[physics.data-an\]](#).
- [36] Travis S. Humble, Andrea Delgado, Raphael Pooser, Christopher Seck, Ryan Bennink, Vicente Leyton-Ortega, C. C. Joseph Wang, Eugene Dumitrescu, Titus Morris, Kathleen Hamilton, Dmitry Lyakh, Prasanna Date, Yan Wang, Nicholas A. Peters, Katherine J. Evans, Marcel Demarteau, Alex McCaskey, Thien Nguyen, Susan Clark, Melissa Reville, Alberto Di Meglio, Michele Grossi, Sofia Vallecorsa, Kerstin Borrás, Karl Jansen, and Dirk Krücker, “Snowmass white paper: Quantum computing systems and software for high-energy physics research,” (2022), [arXiv:2203.07091 \[quant-ph\]](#).
- [37] Christian W. Bauer *et al.*, “Quantum Simulation for High-Energy Physics,” *PRX Quantum* **4**, 027001 (2023), [arXiv:2204.03381 \[quant-ph\]](#).
- [38] Simon Catterall *et al.*, “Report of the Snowmass 2021 Theory Frontier Topical Group on Quantum Information Science,” in *Snowmass 2021* (2022) [arXiv:2209.14839 \[quant-ph\]](#).
- [39] M. Sohaib Alam *et al.*, “Quantum computing hardware for HEP algorithms and sensing,” in *Snowmass 2021* (2022) [arXiv:2204.08605 \[quant-ph\]](#).
- [40] Xiaozhen Ge, Re-Bing Wu, and Herschel Rabitz, “The optimization landscape of hybrid quantum–classical algorithms: From quantum control to NISQ applications,” *Annual Reviews in Control* **54**, 314–323 (2022), [arXiv:2201.07448 \[quant-ph\]](#).
- [41] Adam Callison and Nicholas Chancellor, “Hybrid quantum-classical algorithms in the noisy intermediate-

- scale quantum era and beyond,” *Phys. Rev. A* **106**, 010101 (2022), [arXiv:2207.06850 \[quant-ph\]](#).
- [42] Roberto Campos, *Hybrid Quantum-Classical Algorithms*, Ph.D. thesis, Unlisted (2024), [arXiv:2406.12371 \[quant-ph\]](#).
- [43] T. Lanting, A. J. Przybysz, A. Yu. Smirnov, F. M. Spedalieri, M. H. Amin, A. J. Berkley, R. Harris, F. Altomare, S. Boixo, P. Bunyk, N. Dickson, C. Enderud, J. P. Hilton, E. Hoskinson, M. W. Johnson, E. Ladizinsky, N. Ladizinsky, R. Neufeld, T. Oh, I. Perminov, C. Rich, M. C. Thom, E. Tolkacheva, S. Uchaikin, A. B. Wilson, and G. Rose, “Entanglement in a quantum annealing processor,” *Phys. Rev. X* **4**, 021041 (2014).
- [44] Sukin Sim, Peter D. Johnson, and Alán Aspuru-Guzik, “Expressibility and entangling capability of parameterized quantum circuits for hybrid quantum-classical algorithms,” *Advanced Quantum Technologies* **2** (2019), [10.1002/qute.201900070](#).
- [45] Yuxuan Du, Min-Hsiu Hsieh, Tongliang Liu, and Dacheng Tao, “Expressive power of parametrized quantum circuits,” *Physical Review Research* **2** (2020), [10.1103/physrevresearch.2.033125](#).
- [46] Amira Abbas, David Sutter, Christa Zoufal, Aurelien Lucchi, Alessio Figalli, and Stefan Woerner, “The power of quantum neural networks,” *Nature Computational Science* **1**, 403–409 (2021).
- [47] Samuel Yen-Chi Chen, Shinjae Yoo, and Yao-Lung L. Fang, “Quantum long short-term memory,” (2020), [arXiv:2009.01783 \[quant-ph\]](#).
- [48] Samuel Yen-Chi Chen, Tzu-Chieh Wei, Chao Zhang, Haiwang Yu, and Shinjae Yoo, “Quantum convolutional neural networks for high energy physics data analysis,” (2020), [arXiv:2012.12177 \[cs.LG\]](#).
- [49] Samuel Yen-Chi Chen, Tzu-Chieh Wei, Chao Zhang, Haiwang Yu, and Shinjae Yoo, “Hybrid quantum-classical graph convolutional network,” (2021), [arXiv:2101.06189 \[cs.LG\]](#).
- [50] Marçal Comajoan Cara *et al.*, “Quantum Vision Transformers for Quark–Gluon Classification,” *Axioms* **13**, 323 (2024), [arXiv:2405.10284 \[quant-ph\]](#).
- [51] Eyup B. Unlu *et al.*, “Hybrid Quantum Vision Transformers for Event Classification in High Energy Physics,” *Axioms* **13**, 187 (2024), [arXiv:2402.00776 \[quant-ph\]](#).
- [52] Roy T. Forestano *et al.*, “A Comparison between Invariant and Equivariant Classical and Quantum Graph Neural Networks,” *Axioms* **13**, 160 (2024), [arXiv:2311.18672 \[quant-ph\]](#).
- [53] Zhongtian Dong *et al.*, “ $\mathbb{Z}_2 \times \mathbb{Z}_2$ Equivariant Quantum Neural Networks: Benchmarking against Classical Neural Networks,” *Axioms* **13**, 188 (2024), [arXiv:2311.18744 \[quant-ph\]](#).
- [54] A. Hammad, Kyoungchul Kong, Myeonghun Park, and Soyoung Shim, “Quantum Metric Learning for New Physics Searches at the LHC,” (2023), [arXiv:2311.16866 \[hep-ph\]](#).
- [55] Gary Kochenberger, Jin-Kao Hao, Fred Glover, Mark Lewis, Zhipeng Lü, Haibo Wang, and Yang Wang, “The unconstrained binary quadratic programming problem: a survey,” *Journal of Combinatorial Optimization* **28**, 58–81 (2014).
- [56] Fred Glover, Gary Kochenberger, and Yu Du, “Quantum Bridge Analytics I: a tutorial on formulating and using QUBO models,” *4OR* **17**, 335–371 (2019), [arXiv:1811.11538 \[cs.DS\]](#).
- [57] Andrew Lucas, “Ising formulations of many NP problems,” *Front. in Phys.* **2**, 5 (2014), [arXiv:1302.5843 \[cond-mat.stat-mech\]](#).
- [58] Atanu Rajak, Sei Suzuki, Amit Dutta, and Bikas K. Chakrabarti, “Quantum annealing: an overview,” *Philosophical Transactions of the Royal Society A: Mathematical, Physical and Engineering Sciences* **381** (2022), [10.1098/rsta.2021.0417](#).
- [59] Sheir Yarkoni, Elena Raponi, Thomas Bäck, and Sebastian Schmitt, “Quantum annealing for industry applications: introduction and review,” *Rept. Prog. Phys.* **85**, 104001 (2022), [arXiv:2112.07491 \[quant-ph\]](#).
- [60] Leo Zhou, Sheng-Tao Wang, Soonwon Choi, Hannes Pichler, and Mikhail D. Lukin, “Quantum Approximate Optimization Algorithm: Performance, Mechanism, and Implementation on Near-Term Devices,” *Phys. Rev. X* **10**, 021067 (2020), [arXiv:1812.01041 \[quant-ph\]](#).
- [61] J. Alwall, R. Frederix, S. Frixione, V. Hirschi, F. Maltoni, O. Mattelaer, H. S. Shao, T. Stelzer, P. Torrielli, and M. Zaro, “The automated computation of tree-level and next-to-leading order differential cross sections, and their matching to parton shower simulations,” *JHEP* **07**, 079 (2014), [arXiv:1405.0301 \[hep-ph\]](#).
- [62] Dipsikha Debnath, Doojin Kim, Jeong Han Kim, Kyoungchul Kong, and Konstantin T. Matchev, “Resolving Combinatorial Ambiguities in Dilepton $t\bar{t}$ Event Topologies with Constrained M_2 Variables,” *Phys. Rev. D* **96**, 076005 (2017), [arXiv:1706.04995 \[hep-ph\]](#).
- [63] Ville Bergholm *et al.*, “PennyLane: Automatic differentiation of hybrid quantum-classical computations,” (2018), [arXiv:1811.04968 \[quant-ph\]](#).
- [64] Diederik P. Kingma and Jimmy Ba, “Adam: A Method for Stochastic Optimization,” (2014) [arXiv:1412.6980 \[cs.LG\]](#).
- [65] Daniel Rehfeldt, Thorsten Koch, and Yuji Shinano, “Faster exact solution of sparse maxcut and qubo problems,” (2022), [arXiv:2202.02305 \[math.OC\]](#).
- [66] Gavin E. Crooks, “Performance of the Quantum Approximate Optimization Algorithm on the Maximum Cut Problem,” (2018), [arXiv:1811.08419 \[quant-ph\]](#).
- [67] Leo Zhou, Sheng-Tao Wang, Soonwon Choi, Hannes Pichler, and Mikhail D. Lukin, “Quantum approximate optimization algorithm: Performance, mechanism, and implementation on near-term devices,” *Physical Review X* **10** (2020), [10.1103/physrevx.10.021067](#).
- [68] Stuart Hadfield, Zhihui Wang, Bryan O’Gorman, Eleanor Rieffel, Davide Venturelli, and Rupak Biswas, “From the quantum approximate optimization algorithm to a quantum alternating operator ansatz,” *Algorithms* **12**, 34 (2019).
- [69] Rebekah Herrman, Phillip C. Lotshaw, James Ostrowski, Travis S. Humble, and George Siopsis, “Multi-angle quantum approximate optimization algorithm,” (2021), [arXiv:2109.11455 \[quant-ph\]](#).
- [70] V. Vijendran, Aritra Das, Dax Enshan Koh, Syed M. Assad, and Ping Koy Lam, “An expressive ansatz for low-depth quantum optimisation,” (2023), [arXiv:2302.04479 \[quant-ph\]](#).
- [71] Andrea Skolik, Michele Cattelan, Sheir Yarkoni, Thomas Bäck, and Vedran Dunjko, “Equivariant quantum circuits for learning on weighted graphs,” *npj Quantum Inf.* **9**, 47 (2023), [arXiv:2205.06109 \[quant-ph\]](#).
- [72] Johannes Jakob Meyer, Marian Mularski, Elies Gil-Fuster, Antonio Anna Mele, Francesco Arzani, Alissa

- Wilms, and Jens Eisert, “Exploiting Symmetry in Variational Quantum Machine Learning,” *PRX Quantum* **4**, 010328 (2023), [arXiv:2205.06217 \[quant-ph\]](#).
- [73] Alicia B. Magann, Kenneth M. Rudinger, Matthew D. Grace, and Mohan Sarovar, “Feedback-based quantum optimization,” *Physical Review Letters* **129** (2022), 10.1103/physrevlett.129.250502.
- [74] Alicia B. Magann, Kenneth M. Rudinger, Matthew D. Grace, and Mohan Sarovar, “Lyapunov-control-inspired strategies for quantum combinatorial optimization,” *Physical Review A* **106** (2022), 10.1103/physreva.106.062414.
- [75] Alicia B. Magann, Kenneth M. Rudinger, Matthew D. Grace, and Mohan Sarovar, “Lyapunov-control-inspired strategies for quantum combinatorial optimization,” *Phys. Rev. A* **106**, 062414 (2022), [arXiv:2108.05945 \[quant-ph\]](#).
- [76] Lucas T. Brady and Stuart Hadfield, “FOCQS: Feedback Optimally Controlled Quantum States,” (2024), [arXiv:2409.15426 \[quant-ph\]](#).
- [77] Rajesh K. Malla, Hiroki Sukeno, Hongye Yu, Tzu-Chieh Wei, Andreas Weichselbaum, and Robert M. Konik, “Feedback-based Quantum Algorithm Inspired by Counterdiabatic Driving,” (2024), [arXiv:2401.15303 \[quant-ph\]](#).
- [78] Salahuddin Abdul Rahman, Özkan Karabacak, and Rafal Wisniewski, “Feedback-Based Quantum Algorithm for Constrained Optimization Problems,” (2024), [arXiv:2406.08169 \[quant-ph\]](#).
- [79] I Loshchilov, “Decoupled weight decay regularization,” arXiv preprint [arXiv:1711.05101](#) (2017).
- [80] Xia Liu, Huan Yang, and Li Yang, “Minimizing CNOT-count in quantum circuit of the extended Shor’s algorithm for ECDLP,” (2023), [arXiv:2305.11410 \[quant-ph\]](#).
- [81] Ketan N Patel, Igor L Markov, and John P Hayes, “Efficient synthesis of linear reversible circuits,” arXiv preprint [quant-ph/0302002](#) (2003).
- [82] Phillip C. Lotshaw, Thien Nguyen, Anthony Santana, Alexander McCaskey, Rebekah Herrman, James Ostrowski, George Siopsis, and Travis S. Humble, “Scaling quantum approximate optimization on near-term hardware,” *Sci. Rep.* **12**, 12388 (2022), [arXiv:2201.02247 \[quant-ph\]](#).
- [83] Ruslan Shaydulin *et al.*, “Evidence of scaling advantage for the quantum approximate optimization algorithm on a classically intractable problem,” *Sci. Adv.* **10**, adm6761 (2024), [arXiv:2308.02342 \[quant-ph\]](#).
- [84] Johannes Weidenfeller, Lucia C. Valor, Julien Gacon, Caroline Tornow, Luciano Bello, Stefan Woerner, and Daniel J. Egger, “Scaling of the quantum approximate optimization algorithm on superconducting qubit based hardware,” *Quantum* **6**, 870 (2022), [arXiv:2202.03459 \[quant-ph\]](#).
- [85] J. A. Montanez-Barrera and Kristel Michiels, “Towards a universal QAOA protocol: Evidence of a scaling advantage in solving some combinatorial optimization problems,” (2024), [arXiv:2405.09169 \[quant-ph\]](#).
- [86] M. Cerezo *et al.*, “Variational quantum algorithms,” *Nature Rev. Phys.* **3**, 625–644 (2021), [arXiv:2012.09265 \[quant-ph\]](#).
- [87] Michael A. Nielsen and Isaac L. Chuang, *Quantum Computation and Quantum Information: 10th Anniversary Edition* (Cambridge University Press, 2010).
- [88] Olivier Ezratty, “Is there a Moore’s law for quantum computing?” (2023), [arXiv:2303.15547 \[quant-ph\]](#).
- [89] ATLAS Collaboration, “Performance assumptions for an upgraded ATLAS detector at a High-Luminosity LHC,” (2013).
- [90] Linghua Zhu, Ho Lun Tang, George S. Barron, F. A. Calderon-Vargas, Nicholas J. Mayhall, Edwin Barnes, and Sophia E. Economou, “An adaptive quantum approximate optimization algorithm for solving combinatorial problems on a quantum computer,” (2022), [arXiv:2005.10258 \[quant-ph\]](#).
- [91] Yahui Chai, Yong-Jian Han, Yu-Chun Wu, Ye Li, Menghan Dou, and Guo-Ping Guo, “Shortcuts to the quantum approximate optimization algorithm,” *Physical Review A* **105** (2022), 10.1103/physreva.105.042415.
- [92] P. Chandarana, N. N. Hegade, K. Paul, F. Albarrán-Arriagada, E. Solano, A. del Campo, and Xi Chen, “Digitized-counterdiabatic quantum approximate optimization algorithm,” *Physical Review Research* **4** (2022), 10.1103/physrevresearch.4.013141.
- [93] Jonathan Wurtz and Peter J. Love, “Counterdiabaticity and the quantum approximate optimization algorithm,” *Quantum* **6**, 635 (2022).
- [94] Aditi Misra-Spieldenner, Tim Bode, Peter K. Schumacher, Tobias Stollenwerk, Dmitry Bagrets, and Frank K. Wilhelm, “Mean-field approximate optimization algorithm,” *PRX Quantum* **4** (2023), 10.1103/prxquantum.4.030335.
- [95] Filip B. Maciejewski, Jacob Biamonte, Stuart Hadfield, and Davide Venturelli, “Improving Quantum Approximate Optimization by Noise-Directed Adaptive Remapping,” (2024), [arXiv:2404.01412 \[quant-ph\]](#).
- [96] Vishvesha K. Sridhar, Yanzhu Chen, Bryan Gard, Edwin Barnes, and Sophia E. Economou, “ADAPT-QAOA with a classically inspired initial state,” (2023), [arXiv:2310.09694 \[quant-ph\]](#).
- [97] Nikola Yanakiev, Normann Mertig, Christopher K. Long, and David R. M. Arvidsson-Shukur, “Dynamic-ADAPT-QAOA: An algorithm with shallow and noise-resilient circuits,” (2023), [arXiv:2309.00047 \[quant-ph\]](#).